JOINT TRANSPORTATION
RESEARCH PROGRAM
INDIANA DEPARTMENT OF TRANSPORTATION
AND PURDUE UNIVERSITY

Assessment of Bridges Subjected to Vehicular Collision

Yao Wang

Ashley P. Thrall

SPR-4119 • Report Number: FHWA/IN/JTRP-2019/01• DOI: 10.5703/1288284316870

RECOMMENDED CITATION

Wang, Y., & Thrall, A. P. (2019). *Assessment of bridges subjected to vehicular collision* (Joint Transportation Research Program Publication No. FHWA/IN/JTRP-2019/01). West Lafayette, IN: Purdue University. https://doi.org/10.5703/1288284316870

AUTHORS

Yao Wang
Graduate Research Assistant
Department of Civil & Environmental Engineering & Earth Sciences
University of Notre Dame

Ashley P. Thrall, PhD
Myron & Rosemary Noble Associate Professor of Structural Engineering
Department of Civil & Environmental Engineering & Earth Sciences
University of Notre Dame
(574) 631-2533
athrall@nd.edu
Corresponding Author

JOINT TRANSPORTATION RESEARCH PROGRAM

The Joint Transportation Research Program serves as a vehicle for INDOT collaboration with higher education institutions and industry in Indiana to facilitate innovation that results in continuous improvement in the planning, design, construction, operation, management and economic efficiency of the Indiana transportation infrastructure. https://engineering.purdue.edu/JTRP/index_html

Published reports of the Joint Transportation Research Program are available at http://docs.lib.purdue.edu/jtrp/.

NOTICE

COPYRIGHT

TECHNICAL REPORT DOCUMENTATION PAGE

1. Report No. FHWA/IN/JTRP-2019/01	**2. Government Accession No.**	**3. Recipient's Catalog No.**
4. Title and Subtitle Assessment of Bridges Subjected to Vehicular Collision		**5. Report Date** January 2019 **6. Performing Organization Code**
7. Author(s) Yao Wang and Ashley P. Thrall		**8. Performing Organization Report No.** FHWA/IN/JTRP-2019/01
9. Performing Organization Name and Address Joint Transportation Research Program (SPR) Hall for Discovery and Learning Research (DLR), Suite 204 207 S. Martin Jischke Drive West Lafayette, IN 47907		**10. Work Unit No.** **11. Contract or Grant No.** SPR-4119
12. Sponsoring Agency Name and Address Indiana Department of Transportation State Office Building 100 North Senate Avenue Indianapolis, IN 46204		**13. Type of Report and Period Covered** Final Report **14. Sponsoring Agency Code**

15. Supplementary Notes

Conducted in cooperation with the U.S. Department of Transportation, Federal Highway Administration.

16. Abstract

Vehicles often collide with bridges. However, there are no available guidelines for bridge inspectors to assess damage and to make repair decisions. This project addresses this gap by investigating the behavior of steel girder bridges subjected to vehicular collision through (1) performing non-destructive field testing, (2) developing validated numerical models, and (3) performing parametric investigations to extend research findings. Field testing was performed using Digital Image Correlation (DIC)—a portable, non-destructive, photographic measurement technique that can measure three-dimensional strains based on pattern recognition. Ultimately, the project culminated in assessment guidelines for bridge inspectors to evaluate damaged bridges for repair. This project can benefit Indiana Department of Transportation (INDOT) business processes by potentially reducing the number or amount of repairs, leading to direct cost savings and longer lifespans for bridges

17. Key Words vehicular collision, non-destructive testing, digital image correlation	**18. Distribution Statement** No restrictions. This document is available through the National Technical Information Service, Springfield, VA 22161.

19. Security Classif. (of this report) Unclassified	**20. Security Classif. (of this page)** Unclassified	**21. No. of Pages** 39	**22. Price**

Form DOT F 1700.7 (8-72) Reproduction of completed page authorized

EXECUTIVE SUMMARY

ASSESSMENT OF BRIDGES SUBJECTED TO VEHICULAR COLLISION

Introduction

Vehicles often collide with bridges. However, there are no available guidelines for bridge inspectors to assess damage and make repair decisions. This project addresses this gap by investigating the behavior of steel girder bridges subjected to vehicular collision through (1) performing non-destructive field testing, (2) developing validated numerical models, and (3) performing parametric investigations to extend research findings. Field testing was performed using digital image correlation (DIC)—a portable, non-destructive photographic measurement technique. The focus was on two- and three-span continuous multi-girder steel bridges in which an exterior girder had sustained Category T damage (i.e., torsion about the longitudinal direction). This project can benefit the Indiana Department of Transportation (INDOT) by potentially reducing the number of repairs, leading to cost savings and longer lifespans for bridges.

Findings

- DIC is a powerful monitoring technique that can provide full-field measurements to understand system behavior and capture strain gradients.
- Pressure-activated adhesive tape (with a 10-year or more durability) has been qualified as a DIC pattern strategy to monitor strains in coated steel bridges. This approach can be implemented more rapidly than conventional approaches to reduce the required time for lane closures, leading to cost savings and safety benefits. This has enabled the successful use of DIC in field monitoring for this project.
- DIC, combined with finite element numerical modeling, can provide a better understanding of bridge behavior.
- The measured strains in all girders, subjected to quasi-static dump truck loads, are small (less than 0.022%), demonstrating conservatism in design.
- Loads are generally redistributed away from damaged girders to adjacent girders and rail. This is an area for future research.
- Vehicular collision may damage the shear connectivity between the deck and the damaged girder in composite bridges.
- Cracked or damaged railings may cause positive moment (i.e., tension in the bottom flange) redistribution, resulting in higher strains in damaged girders.
- Damage at the center of a span with a large web rotation angle results in the greatest loss of stiffness compared to other locations and smaller rotation angles.
- Load redistribution in multi-girder bridges and continuity generally reduce safety issues for Category T damage to exterior girders from vehicular collision. However, bridge inspectors must evaluate the potential for this load redistribution when assessing the safety of damaged bridges.

Implementation

This research culminated in *Recommendations for Bridge Inspectors for Evaluating Steel Girder Bridges Subjected to Vehicular Damage* (see Appendix). This will be made available on the INDOT website and will be considered in the upcoming rewrite of the *Indiana Bridge Inspection Manual*. Findings and recommendations were presented at the INDOT Bridge Inspector Workshop on February 13, 2019 (presentation will be available online for one year), the 2019 Purdue Road School, and the INDOT/Joint Transportation Research Program Poster Session on February 13, 2019. To further investigate rail participation, a new project, *Evaluating Reserve Strength of Girder Bridges due to Bridge Rail Load Shedding* (SPR-4311), has been awarded (beginning January 2019).

CONTENTS

LIST OF TABLES

LIST OF FIGURES

1. INTRODUCTION

The aim of this project is to understand the impact of vehicular collision on the behavior of steel girder bridges. Research included (1) performing non-destructive field-testing, (2) developing validated numerical models, and (3) performing parametric investigations to extend research findings. Field testing was performed using digital image correlation (DIC, Figure 1.1)—a portable, non-destructive, photographic measurement technique that can measure full-field three-dimensional (3D) strains. The focus was on two- and three-span continuous multi-girder steel bridges for which an exterior girder has sustained Category T damage, i.e., torsion about the longitudinal direction, as shown for example in Figure 1.2 (FHWA, 2015). The project culminates in recommendations for bridge inspectors to evaluate damaged bridges for repair. This project can benefit Indiana Department of Transportation (INDOT) business processes by potentially reducing the number or amount of repairs, leading to cost savings and longer lifespans for bridges. While this research focused on bridges in Indiana, the results of this study could influence bridge inspection nationally.

Vehicles often collide with bridges, and the frequency and severity of these collisions is increasing (Langfield, 2013). For steel girder bridges, damage is categorized as: (1) strong or major axis bending (Category S), (2) weak or minor axis bending (Category W), (3) torsion about the longitudinal axis (Category T), and (4) local damage including flange bulges and web buckles (Category L) (Figure 1.3). Events typically cause damage that is as a combination of these categories (FHWA, 2015). Category T and L damage is most frequently observed for composite bridges, while Category W and L is more likely for non-composite bridges (Varma & Kowalkowski, 2004). After damage, an engineer must determine if repair is necessary, and if so, what type of repair should be performed (FHWA, 2015). There are currently no available guidelines for bridge inspectors to assess damage and to make repair decisions.

Heat straightening is a common rehabilitation strategy for damaged girders as it is inexpensive, efficient, and enables in-situ repair, which can be performed without shoring (FHWA, 2015; Varma & Sohn, 2013). However, the Federal Highway Administration (FHWA) limits damaged members from being heat straightened more than two times due to loss in ductility of members subjected to multiple damage/repair cycles (FHWA, 2015; Connor, Urban, & Kaufmann, 2008). Reducing the frequency of this repair can extend the lifespan of a bridge or reduce the frequency of girder replacement.

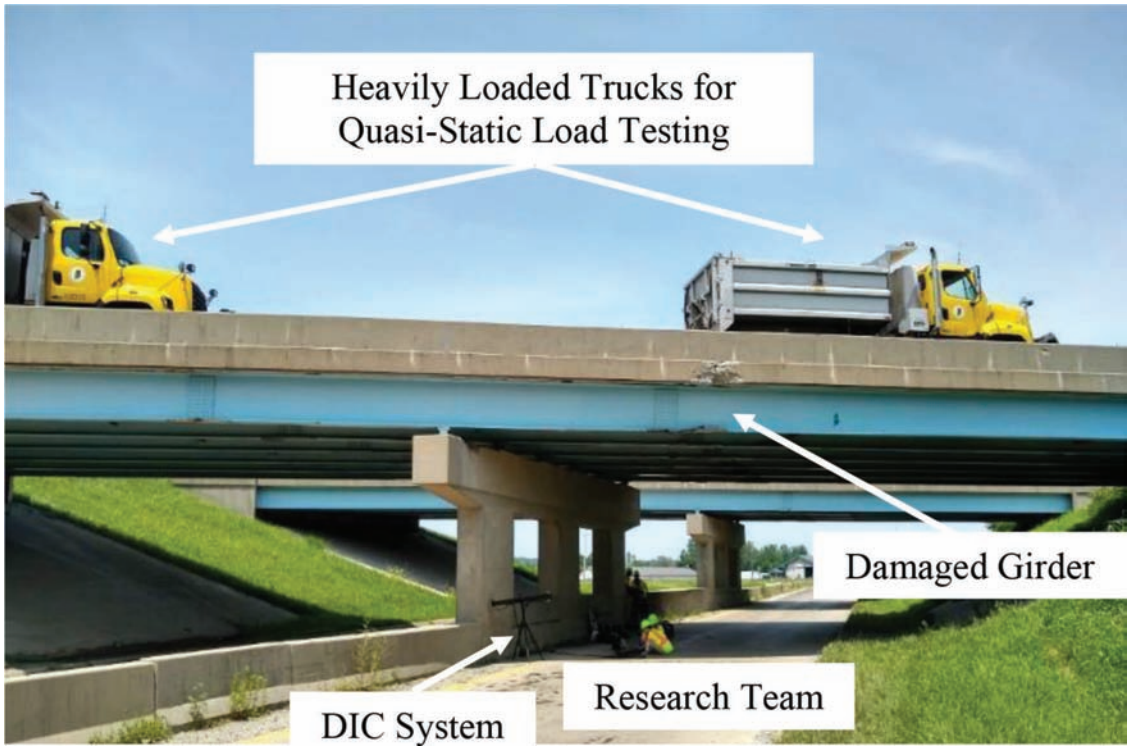

Figure 1.1 Field monitoring using DIC.

Figure 1.2 Damage to steel girders in the four bridges tested in this project.

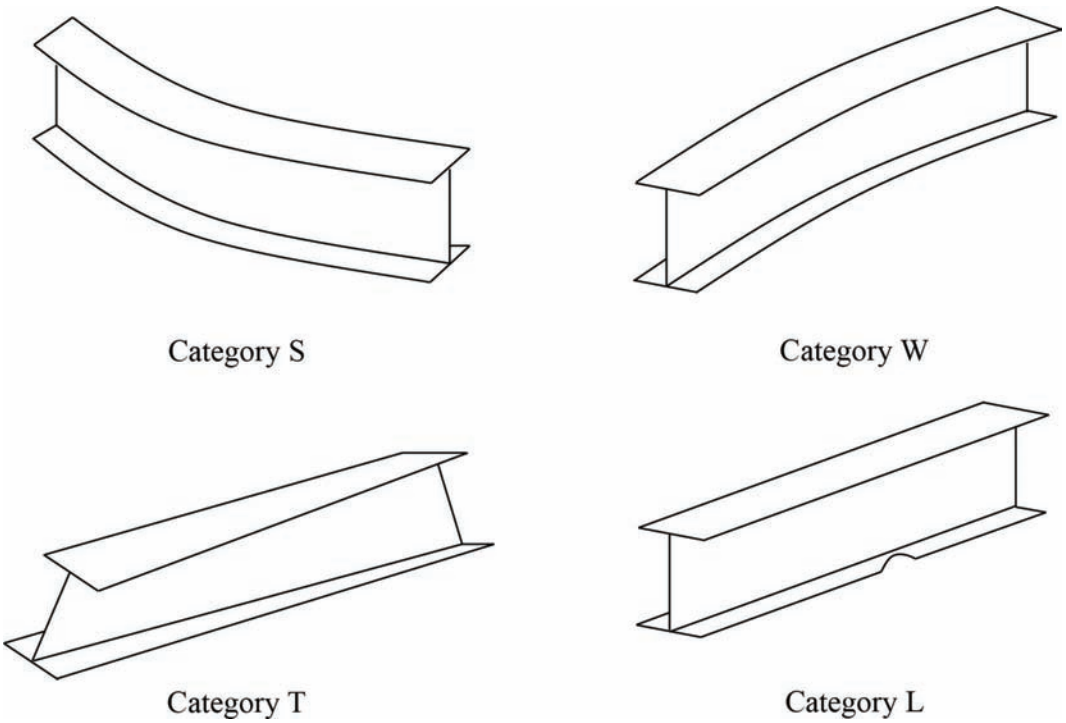

Figure 1.3 Categories of damage (adapted from FHWA, 2015).

2. BACKGROUND

2.1 Behavior of Bridges Subjected to Vehicular Collison

There is little existing research on the behavior of steel girder bridges that have been subjected to collision damage. The most relevant research is focused on heat straightening severely damaged steel girders as opposed to assessing damaged members.

Heat straightening dates back to early welders (FHWA, 2015) and has been performed on bridges since the mid-20th century (Avent, Robinson, Madan & Shenoy, 1992; Avent, 1989). However, little research had been performed in this area until the 1970s and 1980s (FHWA, 2015; Lackowski & Varma, 2007). Avent et al. (1992) performed the first experimental study to investigate the effect of heat straightening on initially damaged specimens, finding that damaged specimens with strains up to 100 times yield strain could be heat straightened. Earlier experimental research focused on the behavior of undamaged steel subjected to heat treatment (Lackowski & Varma, 2007). The reader is referred to Lackwoski & Varma (2007) for a detailed review of research related to heat straightening. Recent major research activity in this area includes the work of Varma & Kowalkowski (2004) who investigated the effect of damage strain, remaining stress, damage/repair cycles, and heating temperature on material properties. A recent study into the fatigue and fracture performance of heat-straightened steel bridge girders by Conner et al. (2008) found that the recommended number of damage/repair cycles should be limited to two (as had previously been found by prior research and was recommended in FHWA guidelines). This work also developed guidelines on heat straightening, including recommendations on treatment of an area prior to repair and on the magnitude of the restraining force. As heat straightening in the field does not necessarily follow the guidelines of the FHWA (FHWA, 2015), Varma & Sohn (2013) have investigated the effect of "realistic" heat straightening on beam capacity. While research in heat-straightening repairs of steel girders damaged by collision is mature, there is a major research gap in understanding the behavior of girders damaged by collision.

2.2 Digital Image Correlation for Bridge Monitoring

Non-destructive monitoring of bridges is critical to assess the structural condition of existing bridges and to inform the design of new structures. Conventional approaches to monitoring strains and displacements in structures (i.e., using strain gauges and linear displacement transducers) are limited as the sensors are only capable of taking measurements at specific locations in directions selected a priori, must be continuously taking measurements, and require an on-site data acquisition system. Alternatively, DIC—a photographic measurement technique that relies on pattern recognition to calculate displacements and strains (Sutton, Orteu & Schreier, 2009; Schmidt, Tyson, & Galanulis, 2003)—can provide full-field measurements to understand

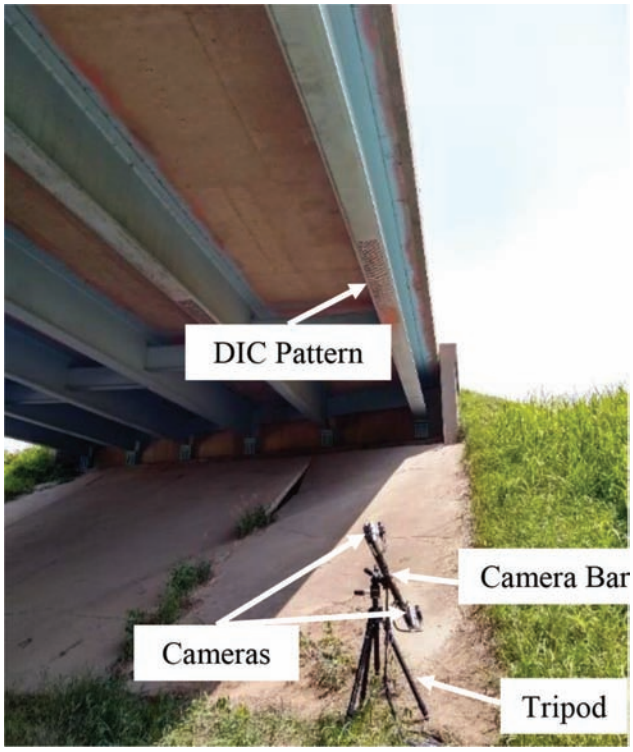

Figure 2.1 DIC system being used in the field.

system behavior and capture strain gradients (in post-processing, strain can be calculated in any direction to understand strain gradients or investigate strains in varying directions). This portable technique can take measurements continuously for short-term monitoring and can take discrete measurements at varying times to capture long-term behavior (without requiring on-site hardware in the interim). Because of these advantages, this project uses 3D DIC to non-destructively test steel girder bridges that have been subjected to vehicular impact.

A 3D DIC system (Figure 2.1) consists of two cameras mounted on a tripod, which measure surface displacements and strains of a sample within the "field-of-view" (FOV). A sample must be prepared with a random pattern (e.g., ellipses or lines to achieve greyscale variation). Stereo pairs of photographs are captured before, during, and after loading. The captured digital images are divided into pixelated regions called facets. Using pattern recognition and photogrammetric triangulation principles, these facets are tracked through a complete image series to yield full-field 3D displacements and strains. For the DIC system used for this research, displacements can be measured with an accuracy of 1/30,000 of the FOV (Schmidt et al., 2003; e.g., for a 6 ft. wide girder section, the accuracy is up to 0.0024 in.).

While DIC can provide unprecedented near full-field data on bridge behavior, there are many challenges associated with implementing it in the field. Inclement weather, particularly rain, poses a problem for DIC as precipitation in the photographs may interfere with

pattern recognition (Bell, Peddle, & Goudreau, 2012) and potentially damage exposed hardware. A minimum amount of light is required (Bell, Gaylord, Goudreau, & White, 2015) and solar glare should be avoided (Bell et al., 2012; Peddle, Goudreau, Carlson, & Santini-Bell, 2011). The measurement area is limited by the FOV of the cameras (Busca, Cigada, Mazzoleni, & Zappa, 2014). Controlling the position and angle of the cameras may be challenging in the field due to natural or man-made obstructions, which may adversely impact resolution of data or the FOV (Bell et al., 2015). Commercially available DIC systems tend to be expensive (Busca et al., 2014). Measuring small strains can be challenging, as the reported strain accuracy of the system used in this research is less than 0.01% (ARAMIS, 2013).

There have been limited applications of DIC for bridge monitoring. Yoneyama, Kitagawa, Iwata, Tani & Kikuta (2007) used DIC to measure deflections of a steel girder bridge during load tests. They compared DIC measurements with that of displacement transducers, finding good agreement. This research was performed in two dimensions (2D) with single cameras (as opposed to 3D using pairs of cameras). Bell et al. (2012) and Peddle et al. (2011) used 2D DIC to measure the behavior of a continuous steel girder bridge and a concrete culvert retrofitted with fiber reinforced polymer reinforcement. DIC measurements were compared with results from linear variable displacement transducers, finding close agreement. The New Hampshire Department of Transportation funded a recent project titled "Instrumentation, Digital Image Correlation, and Modeling to Monitor Bridge Behavior and Condition Assessment" to investigate the behavior of a composite steel girder bridge using 2D DIC (Bell et al., 2015). Displacements under a load test were measured and used to evaluate the continuous behavior of the bridge. Other applications for field monitoring bridges using DIC include measuring displacements of steel girder bridges under truck loading (Chiang, Shih, Chen, & Yu, 2011), displacements and vibrations of railroad bridges subjected to train loads (Hoag, Hoult, Take, & Le, 2015; Busca et al., 2014) and tension and dynamic characteristics of hanger cables (Kim & Kim, 2013). Among other applications, are the local effects of bridge components (i.e., riveted girders, stay cable anchorages, steel plates in a box girder), global effects of a multi-span twin steel box bridge (Winkler, Hendy, & Waterfall, 2015) and field spalling, crack size, and long-term strain of concrete bridge piers (Nonis, Niezrecki, Yu, Ahmed, Su, & Schmidt, 2013). There is no prior research using DIC to study bridges damaged by vehicular collision.

3. PRESSURE ACTIVATED ADHESIVE TAPE PATTERN STRATEGY

3.1 Introduction

Conventionally, DIC patterns are applied by painting a surface white, then applying the grayscale variation by spray paint splatter, drawing lines by marker, or using a brush/stencil (ARAMIS, 2013). These approaches are appropriate for a laboratory. However, they are time-intensive which can become prohibitive for bridge monitoring where pattern application may require work at heights, access equipment, and lane closures. Further, they are weather-dependent and prone to deterioration. While some researchers have used spray paint (Baah, 2014), stencil (Nonis et al., 2013), and paint rollers (Nonis et al., 2013), many have noted the difficulty of implementing these conventional approaches in the field (Bell et al., 2012; Busca et al., 2014; Yoneyama et al., 2007) and have developed alternative approaches, such as affixing targets (Hoag et al., 2015; Bell et al., 2015; Bell et al., 2012; Peddle et al., 2011; Chiang et al., 2011; Busca et al., 2014; Nonis et al., 2013), applying chalk (Peddle et al., 2011), attaching magnets (Yoneyama et al., 2007), and relying on natural surface texture (Yoneyama et al., 2007; Hoag et al., 2015). While these alternative approaches are quick, they can only be used for short-term monitoring and are not capable of measuring full-field strain gradients. An additional challenge in the case of steel bridge structures is that these structures are already treated with a protective multi-layer paint coating. Any DIC pattern must be compatible with the bridge coating system, such that the pattern "follows" the strain in the steel beneath the coating.

To address the challenge of applying DIC patterns to steel bridge structures, this research investigated pressure-activated adhesive tape as a patterning approach. With tape, a durable, large pattern can be applied quickly in varying weather conditions and without removing the protective coating system. The DIC pattern can be designed electronically to minimize noise and printed on the tape prior to installation. A vinyl adhesive tape has previously been investigated for small-scale composite samples (El-Hajjar & Petersen, 2011); however, there is no existing research demonstrating that tape is a viable patterning approach for steel structures, specifically for coated steel structures.

The qualification of the tape patterning approach is a critical component of this research as the monitored bridges for this project are over active traffic and therefore lane closures are required. Minimizing lane closure time is important as it requires extensive support from INDOT maintenance crews and, more importantly, lane closures pose significant safety hazards to the traveling public (Huebschman, Garcia, Bullock, & Abraham, 2003).

This research qualified pressure-activated adhesive tape as a strategy to rapidly apply a DIC pattern on bare and coated steel structures. The capability of the tape to follow strains in steel samples was evaluated through tensile tests. Surface strains on bare and coated steel samples—measured via (1) strain gauges, (2) an extensometer, (3) DIC with spray paint pattern, and (4) DIC with tape pattern—were compared. Further tensile tests were used to investigate strains on bare steel samples with a hole, comparing measured results from DIC with spray paint and tape patterns to predictions from finite element (FE) models.

3.2 Experimental Program

3.2.1 Testing Protocol

Tensile tests were performed using a universal testing machine (UTM) to measure strains as described in Table 3.1. Data for elastic tests (Scenarios A-C) are zeroed when both the top and bottom of samples are clamped in the UTM grips to remove strains induced from clamping from the measurements. For plastic tests (Scenario D), data are zeroed when only the top of the sample is gripped.

3.2.2 Material Testing

ASTM material testing (ASTM 2010a,b; 2014a,b) was performed on the (1) 0.125 in. thick bare steel (Scenarios A and D, 3 specimens), (2) 0.125 in. thick coated steel (Scenario B, measurements taken on uncoated side, 1 specimen), and (3) 0.5 in. thick bare steel (Scenario C, 8 specimens from 2 bars, testing performed in Gerbo, Thrall, Smith, & Zoli [2016]) using 2 in. gauge length coupons at full thickness (Figure 3.1, Table 3.2). An extensometer (2 in. gauge length) measured the longitudinal strain, to calculate the Young's modulus, E and the yield strength, F_y. Stress was calculated based on the measured area of the samples and the force measured by the UTM. Strain gauges (EA-06-125BZ-350/E, MicroMeasurements) measured the longitudinal and transverse strain, to calculate Poisson's ratio, v.

The strain gauge and extensometer data that are presented and compared against DIC data are from these material tests. These conventional sensors would block the DIC cameras and could not be performed simultaneously with DIC.

3.2.3 Digital Image Correlation

Surface strains were measured using a 3D DIC system consisting of two cameras (2448 × 2050 pixels, 1.97 in. lenses). The FOV was 8.67 × 7.07 in. Strains were calculated using ARAMIS (ARAMIS, 2013), with a gauge length of 0.0425 in.

Noise in DIC measurements can be attributed to: (1) image quality (affected by lighting, air turbulence, pattern size/shape, camera-related noise, etc.) or (2)

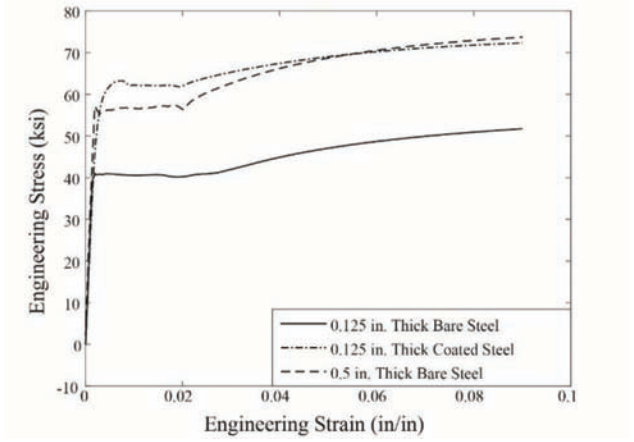

Figure 3.1 Measured engineering stress-strain relationships. (Data from 0.5 in. thick bare steel samples reprinted from *Journal of Constructional Steel Research, 127*, E. J. Gerbo, A. P. Thrall, B. J. Smith, & T. P. Zoli, Full-field Measurement of Residual Strains in Cold Bent Steel Plates, 187–203, 2016, with permission from Elsevier.)

TABLE 3.2
Measured material properties.

	E (ksi)	F_y (ksi)	v
0.125 in. Thick bare steel samples (Scenarios A and D):			
Mean	29,900	40.5	0.280
SD	373	0.546	4.99E-3
COV(%)	1.25	1.35	1.79
0.125 in. Thick bare steel samples (Scenarios B):			
Value	25,900	63.1	0.254
0.5 in. Thick bare steel samples (Scenario C):			
Mean	29,500	56.5	0.280
SD	635	0.887	1.27E-3
COV(%)	2.15	1.57	0.453

SD: standard deviation; COV: coefficient of variation; E: Young's modulus; F_y: yield strength; v: Poisson's ratio.

Data from 0.5 in. thick bare steel samples reprinted from *Journal of Constructional Steel Research, 127*, E. J. Gerbo, A. P. Thrall, B. J. Smith, & T. P. Zoli, Full-field Measurement of Residual Strains in Cold Bent Steel Plates, 187–203, 2016, with permission from Elsevier.

TABLE 3.1
Test summary.

		Nominal sample dimensions		
Testing scenario	**Loading protocol**	t **(in.)**	w **(in.)**	l **(in.)**
A. Longitudinal elastic strain in bare steel	Load control, .250 k/min up to 4 k, load held and DIC data collected every .25 k	0.125	1.00	10.0
B. Longitudinal strain in coated steel	Load control, .250 k/min up to 4 k, load held and DIC data collected every .25 k	0.125	1.00	10.0
C. Transverse strain in bare steel	Load control, 10 k/min up to 100 k, load held and DIC data collected every 25 k	0.500	5.50	17.0
D. Longitudinal plastic strains in bare steel around a hole	Displacement control, 0.15 in./min until breaking, DIC data collected every 2s	0.125	1.00	10.0

t: sample thickness; w: sample width; l: sample length.

correlation processing (e.g., poor calibration, numerical errors) (Baldoni, Lionello, Zama, & Cristofolini, 2016). An effective means of reducing random noise, particularly for a uniform strain distribution, is to use averaging. This can include (1) area averaging, in which the strains over an area are averaged within one DIC frame (where a frame refers to a pair of 3D DIC photographs) and/or (2) time averaging, in which strains are averaged over multiple frames taken in quick succession. In this chapter (unless noted otherwise), data has been processed via both area averaging and time averaging. Specifically, ten frames were analyzed for each load level (i.e., the load was held constant while DIC photographs were taken), with frames taken within 15 seconds of one another. The reported strain value is from averaging both over an area (specified later in the paper) and over ten frames. The full-field strain plots do not include time or area averaging.

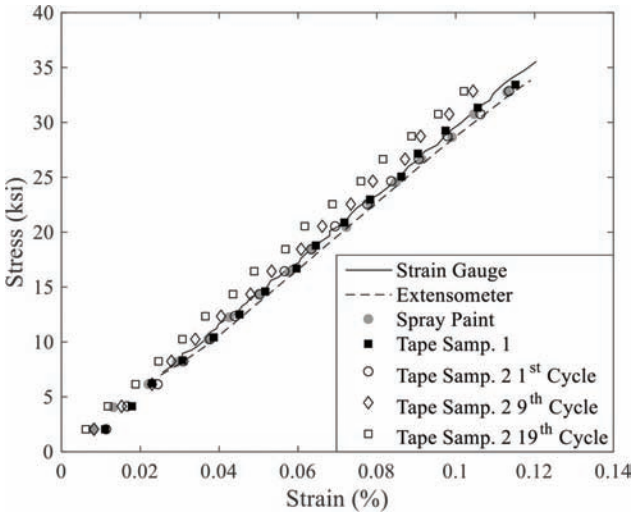

Figure 3.2 Scenario A: Elastic longitudinal stress-strain behavior of 0.125 in. thick bare steel samples.

3.3 Results

3.3.1 Scenario A. Longitudinal Elastic Strains in Bare Steel

Figure 3.2 shows the elastic behavior—measured via strain gauge, extensometer, and DIC with spray paint and tape patterns—for the 0.125 in. thick bare steel samples in Scenario A. One spray paint sample was tested. Four tape samples were tested to demonstrate repeatability (only two samples are shown for clarity). The area over which the DIC results are averaged is 5.0 in. in length by 0.5 in. in width and is indicated by the black dashed region in Figure 3.3. This region excludes (1) noise near pattern edges, which is an artifact of the DIC algorithm, and (2) measurements near the tape edge (0.5 in. as marked by black solid lines in Figure 3.3b, referred to as the development length, discussed later).

Figure 3.2 clearly demonstrates that DIC measurements are able to closely match data reported via conventional instrumentation. Further statistical comparison is made by calculating the percent error between the DIC measurements and the predicted stresses based on the material testing measurements (Table 3.3). The predicted stresses are calculated based

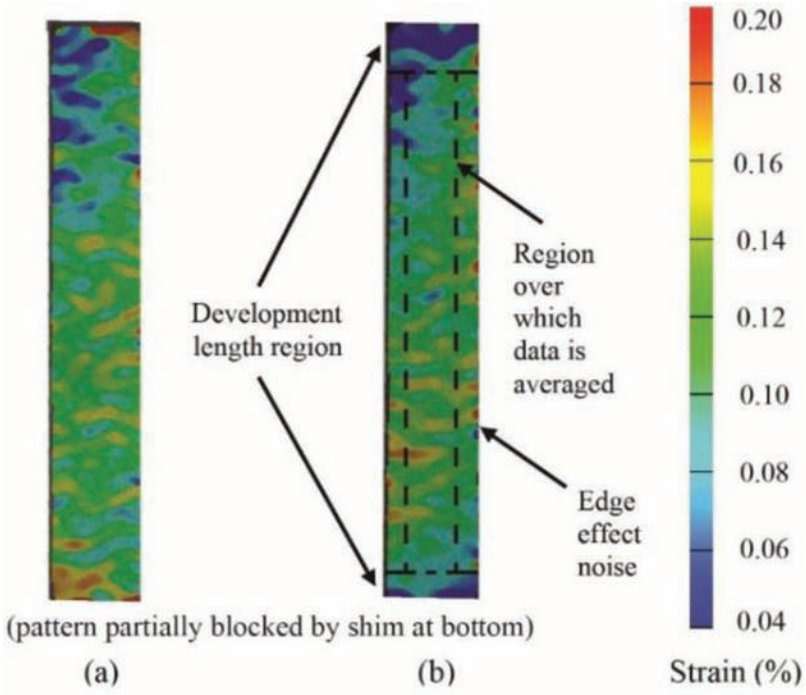

Figure 3.3 Scenario A: Measured full-field DIC longitudinal strains of 0.125 in. thick bare steel samples at a load of 4 k with (a) spray paint pattern and (b) tape pattern.

TABLE 3.3
Measured error.

Testing scenarios		Mean % error	SD	COV
Scenario A	Spray Paint	4.12	2.76	0.670
	Tape Samp. 1	6.09	7.16	1.18
	Tape Samp. 2 1st	6.50	6.56	1.01
	Tape Samp. 2 9th	-0.587	5.24	-8.93
	Tape Samp. 2 19th	-9.29	2.04	-0.220
	Tape Samp. 3	-5.08	3.05	-0.600
	Tape Samp. 4	2.84	2.61	0.920
Scenario B	Spray Paint	3.38	4.29	1.27
	Tape	11.8	10.5	0.889
Scenario C	Spray Paint Samp. 1	-15.2	4.21	-0.277
	Spray Paint Samp. 2	9.40	5.35	0.570
	Spray Paint Samp. 3	27.7	5.36	0.194
	Tape Samp. 1	27.9	6.38	0.229
	Tape Samp. 2	25.3	4.56	0.181
	Tape Samp. 3	-3.35	2.49	-0.745

SD: standard deviation; COV: coefficient of variation.

on the average measured Young's modulus, E in Table 3.2, the load, and the measured cross-sectional properties. The mean percent errors represent the average over the entire loading sequence, neglecting those measurements with strains less than the accuracy of the DIC system (i.e., 0.01% strain). All DIC measurements demonstrate less than 10% mean error compared to the predicted results. Notably, the tape pattern data closely matches that of the spray paint (Figure 3.3), and the mean errors are comparable. The DIC measurements for the four tape samples matched closely, demonstrating repeatability. Tape Sample 2 was cycled (i.e., repeatedly loaded and unloaded using the same loading protocol) 19 times. Results from the 1st, 9th, and 19th cycles are shown in Figure 3.2, demonstrating that the tape's performance does not degrade with cycles. The mean percent error also remains small throughout these cycles (Table 3.3).

Figure 3.3 further demonstrates that the spray paint and tape pattern results in equivalent DIC data by showing the measured full-field longitudinal strains. This figure also shows the noise related to the edge effect in both the spray paint and tape data. Lower measured strains are observed in the development length region of the tape data (to be discussed later).

Overall, these tensile tests demonstrated that the tape pattern follows the strain in bare steel samples, even for small elastic strains (i.e., expected signal range for bridge monitoring).

3.3.2 Scenario B. Longitudinal Elastic Strains in Coated Steel

Analogous measurements were also compared for 0.125 in. thick coated steel samples (Figures 3.4 and 3.5). Two samples were tested: one with spray paint pattern and one with tape. Area averaging in Figure 3.4 uses the same region as Scenario A. Results demonstrate that DIC

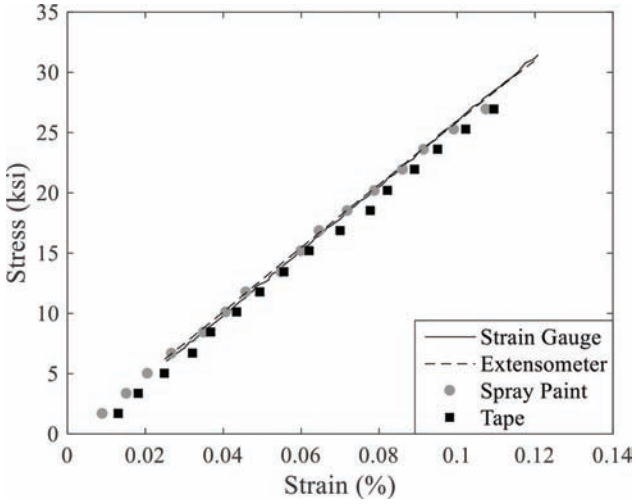

Figure 3.4 Scenario B: Elastic longitudinal stress-strain behavior of 0.125 in. thick coated steel samples.

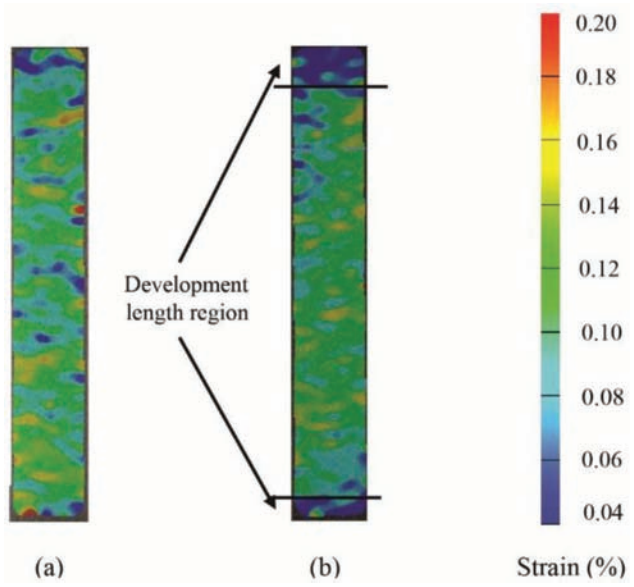

Figure 3.5 Scenario B: Measured full-field DIC longitudinal strains of 0.125 in. thick coated steel samples at a load of 4 k with (a) spray paint pattern and (b) tape pattern.

measurements with both tape and spray pattern are able to closely match that of the conventional instrumentation. The mean percent errors, compared to the predicted values, are low for both specimens (below 12%, Table 3.3). Importantly, the results qualify DIC with tape pattern as an approach for monitoring coated steel bridges. Therefore, monitoring can be performed without removing protective coatings.

3.3.3 Development Length

DIC measurements with the tape pattern are reporting lower longitudinal strains within approximately 0.5 in. of a tape edge (in the direction of the load) compared to the spray paint pattern (Figures 3.3 and 3.5).

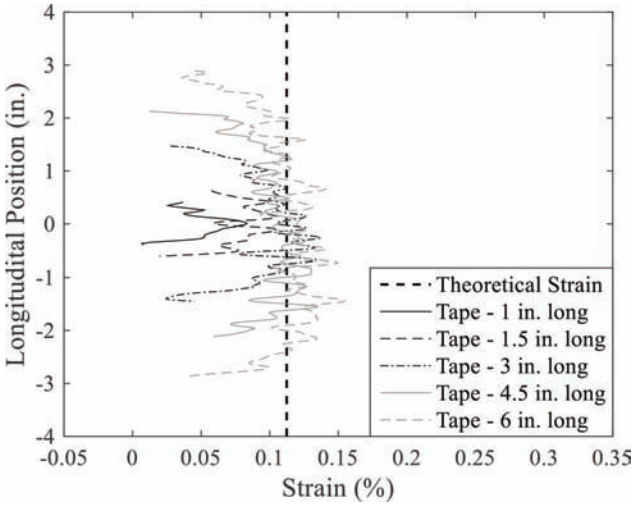

Figure 3.6 Scenario A: Measured elastic longitudinal strain of 0.125 in. thick bare steel samples at a load of 4 k with varying tape lengths.

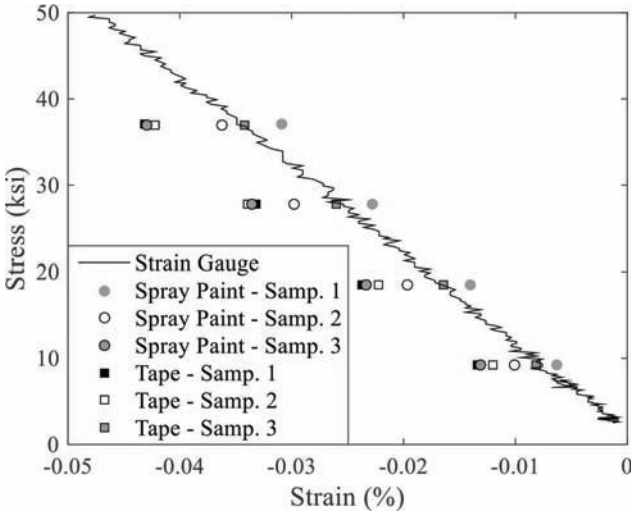

Figure 3.7 Scenario C: Measured elastic transverse stress-strain behavior of 0.5 in. thick bare steel samples.

This can be attributed to the construction of the tape, which is comprised of the following layers: (1) adhesive, (2) white print film, (3) adhesive, and (4) clear film over laminate. As deformations are transferred from the steel to the outer layer, the adhesive deforms more than the film. Therefore, strains measured near the tape edge reflect the behavior of the outer film as opposed to the steel. After a length, the outer film ultimately matches the steel. This length is considered the "development length" of the tape.

The tape in Scenarios A and B is 6 in. long. To quantify the development length of the tape, four additional Scenario A tensile tests were performed with varying tape lengths. The measured longitudinal strain along the length of the sample is shown in Figure 3.6. The predicted theoretical strain (0.111%)—calculated based on the average measured Young's modulus, E, the load, and the average measured cross-sectional properties—is highlighted for reference. For this data, time averaging over 10 frames was used. As this study focuses on strains at particular longitudinal positions along the sample, area averaging is not appropriate. Instead, strains are averaged along the width of the sample for each longitudinal position. The focus is on the middle 0.5 in. width of the sample to eliminate edge effect noise across the width. Edge effects along the length were excluded by removing 0.127 in. of data. This tighter limit is based on a parametric investigation of the edge effect noise and is used for this study. For tape lengths greater than 1.5 in., the measured strain asymptotes toward approximately 0.11% in the middle of the sample at a load of 4 k after the initially lower values in the first 0.5 in. length of tape (measured from the bottom and top of the tape). The 1 in. tape is unable to fully develop.

Based on these results, the development length of this tape is approximately 0.5 in. Data within the development length should be ignored. However, this is not a limitation for bridge monitoring, as the region to be monitored is typically much larger.

3.3.4 Scenario C. Transverse Elastic Strains in Bare Steel

To qualify the tape for elastic strains in compression, transverse strains were also measured in tensile tests (Scenario C). Due to the development length issue, wider samples were used. Three samples were tested, with spray paint on one side and tape on the reverse. Figure 3.7 shows the transverse behavior measured via strain gauge and DIC with spray paint and 5.5 in. wide tape pattern. Area averaging was performed over a 6.0 in. length and 4.5 in. width. DIC results agree well with the conventional instrumentation. The mean errors with respect to the predicted stresses tend be higher than observed in Scenario A (Table 3.3). However, the magnitude of this error is similar for both spray paint and tape specimens. This larger error can be attributed to the small magnitude of strain being measured. DIC measurements exhibit variability across the samples, but this can also be attributed to the small values of strain being measured. Higher noise was observed with the spray paint pattern data (see full-field strains in Figure 3.8). This is due to user difficulty in controlling the size/density of the pattern when applied via spray paint. The tape provides the opportunity for greater pattern control to minimize noise. Overall, these tests demonstrated that the tape is also qualified for compressive strains.

3.3.5 Scenario D. Longitudinal Plastic Strains in Bare Steel

To further qualify the tape, tensile testing was performed on 0.125 in. thick bare steel samples with a machined 0.25 in. diameter hole (Scenario D). Two samples were measured via DIC with spray paint and two samples were measured via DIC with tape pattern. No area or time averaging was implemented.

Measured results were compared with results from a 3D FE model built in ABAQUS/Standard with implicit

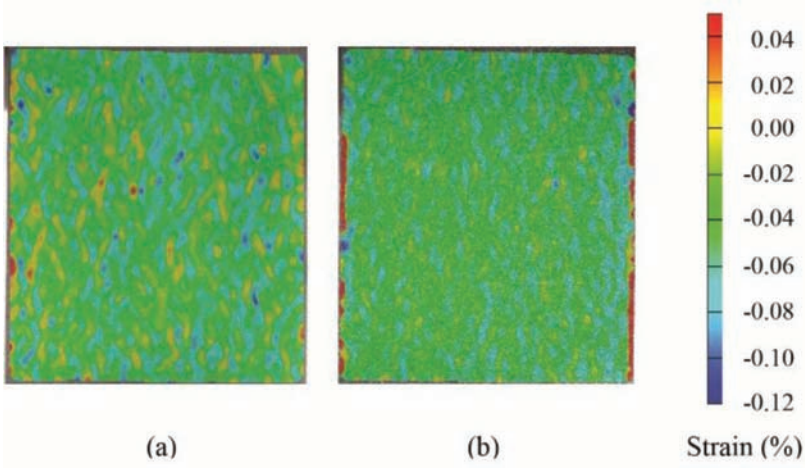

Figure 3.8 Scenario C: Measured DIC full-field transverse strains of 0.5 in. thick bare steel samples at a load of 100 k with (a) spray paint pattern and (b) tape pattern.

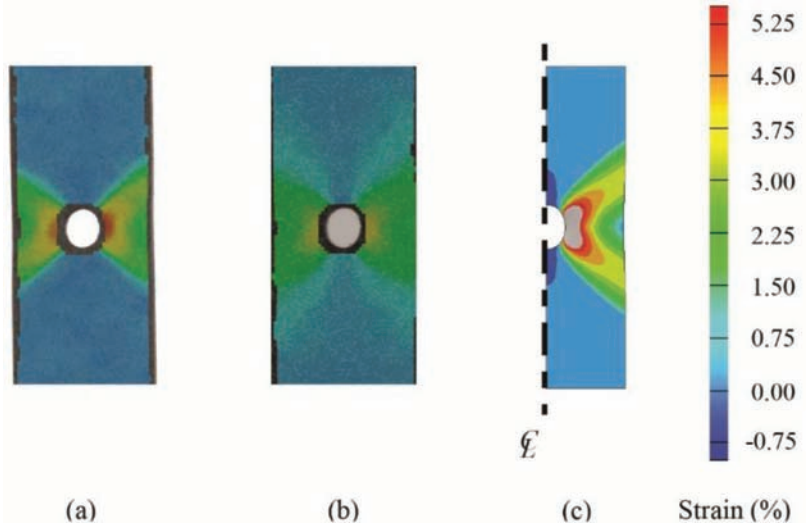

Figure 3.9 Scenario D: Measured full-field longitudinal strains of 0.125 in. thick bare steel samples with 0.25 in. diameter hole at a load of 4.5 k determined by (a) DIC with spray paint pattern, (b) DIC with tape pattern, and (c) FE model (gray indicates strains exceeding the highest value in the color map).

analysis (ABAQUS, 2014). C3D8R solid continuum elements with a mesh size of approximately 0.00625 in. were used. Symmetry was employed about the longitudinal axis. Boundary conditions were implemented to approximate the UTM grips. For the top 1 in., translation in all directions is restrained. For the lower 1 in., translation perpendicular to sample's axis is restrained. The load was applied in the longitudinal direction uniformly across the nodes at the bottom of the sample. The model used nonlinear geometry and a nonlinear material model based on the measured material properties (Table 3.2).

Measured and predicted longitudinal strains were compared at a load for which the peak predicted strain was in the strain-hardening region (Figure 3.9 and Figure 3.10). DIC with both spray paint and tape matched the general trend of strains predicted by the FE model. There is DIC data loss around the hole as a result of the different views of the two cameras (i.e., each camera sees a different part of the hole and edge and therefore the software cannot accurately match patterns in this region), which prevents this technique from measuring the peak strains directly at the hole edge. Differences between the FE model predictions and the measured results can be attributed to the assumed isotropic behavior in the FE model, which is based on ASTM coupons tested in the direction of steel rolling. Therefore, any anisotropies in the steel are not included in the FE predictions. The minor differences between the DIC with spray paint and tape results can be attributed to the tape development length. Toward the edges of the hole, the outer film will not fully follow the strains in the steel underneath. This is noticeable in Figure 3.9 and Figure 3.10 in the region above the hole

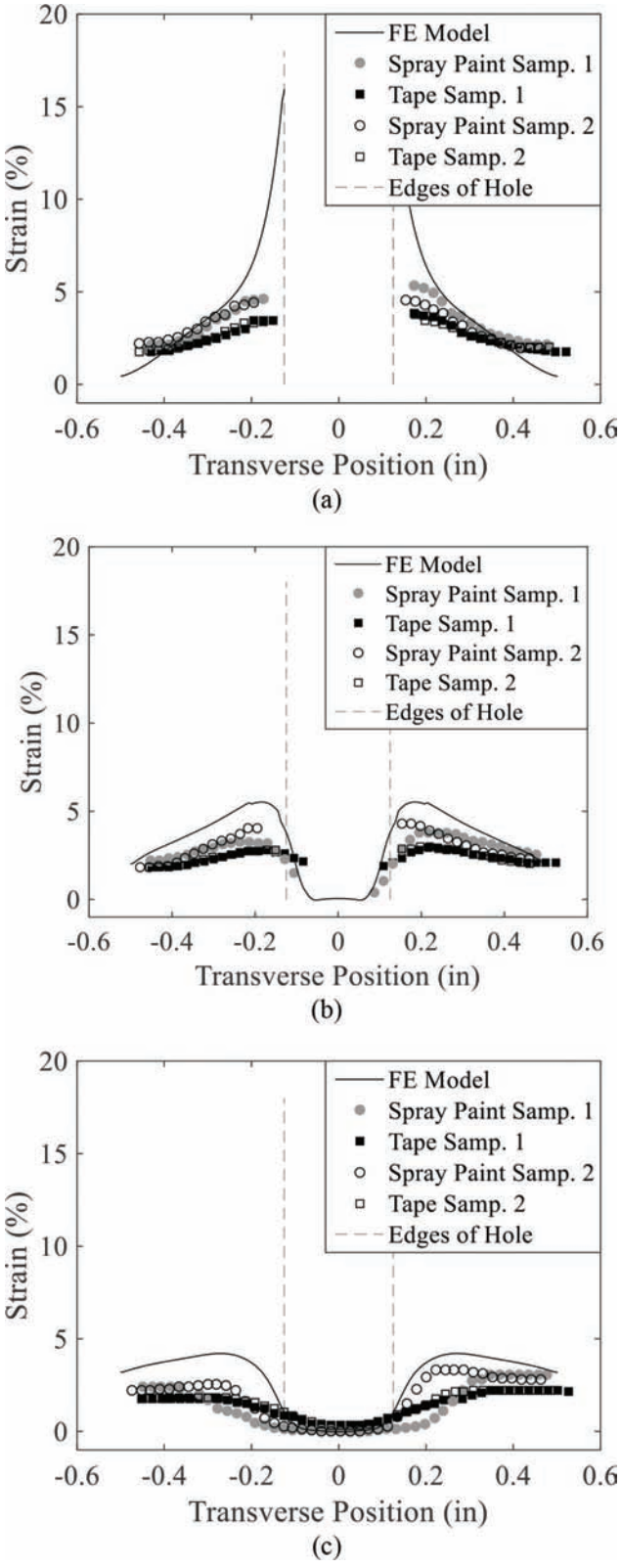

Figure 3.10 Scenario D: Measured longitudinal strains of 0.125 in. thick bare steel samples with 0.25 in. diameter hole at a load of 4.5 k. Measurements are along the sample width, located at (a) the hole center, (b) 0.125 in. above the hole center, and (c) 0.25 in. above the hole center.

where the longitudinal strains measured via DIC with tape pattern are slightly higher than those measured using spray paint. As the tape composite has a much lower stiffness than the steel, it is expected that it would have higher strains in this region prior to achieving the full development length.

3.4 Summary

This chapter has demonstrated that pressure-activated adhesive tape is a viable DIC patterning strategy to monitor coated steel bridges via digital image correlation. A limitation in this approach is that it relies on the coating being intact and bonded to the steel. The coating system should be visually inspected prior to tape installation. If there are signs of coating degradation, the damaged coating should be removed. While this does result in coating removal, the ability to rapidly install the tape provides significant benefit compared to conventional approaches (which would also require coating removal). With this qualification of the tape patterning strategy, this approach was used for all four bridges studied.

4. FIELD MONITORING AND NUMERICAL MODELING

4.1 Field Monitoring Approach

Field monitoring was performed by measuring strains in each bridge under quasi-static truckloads (i.e., two heavily loaded dump trucks). Four bridges with Category T damage were monitored (Figure 1.2). The research proposal planned to monitor six. However, there were few vehicular collisions during the project and there were challenges in obtaining lane closures to monitor damaged bridges due to high traffic volumes. The plan to monitor four bridges was agreed upon by the Business Owner and Principal Investigator. The focus was on monitoring the behavior of exterior damaged girders, symmetric undamaged girders, and adjacent girders. Surface strains were measured using a 3D DIC system consisting of two cameras (2448 × 2050 pixels, 0.472 in. lenses) mounted on a rigid bar (Figure 2.1). Strains were calculated using ARAMIS (2017), with a gauge length of 2.97 in. Specifically, twenty frames were taken within 15 seconds of one another for each load case (i.e., the trucks stayed in place when photographs were taken). Time averaging was implemented using the temporal binomial filter in ARAMIS (2017), averaging data over 10 frames for each load case. The spatial median filter in ARAMIS (2017) was used to reduce outlying data points. Area averaging was also performed, including data across the entire pattern but excluding the 0.5 in. development length of the tape along all edges. Full-field strain maps included in this report feature only temporal and spatial filtering.

4.2 Numerical Modeling Approach

3D FE numerical models were built in ABAQUS/Standard (2018) using implicit analysis. S4R shell elements were used for the steel girders and diaphragms, as well as the concrete decks and rails (where appropriate). The cross-section of the rail was modeled using rectangular shell elements (with centers aligned vertically) which were determined by the points where the thickness of the rail changes. A mesh size of 3 in. was chosen based on results from a mesh refinement study. All models in this chapter remain in the linear material range. The assumed properties for steel include a Young's modulus of 29,000 ksi and Poisson's ratio of 0.3. The linear material model for 4 ksi compressive strength concrete assumes a Young's modulus of 3,950 ksi (calculated according to AASHTO [2017]) and Poisson's ratio of 0.2. Any changes to the steel material properties due to damage from collision were ignored. To approximate composite behavior, the deck was tied to the top flange of the girders (i.e., there was no relative movement between the deck and top flange). To approximate the non-composite behavior, surface-to-surface contact was used between the deck and the top flange of the girders. The coefficient of friction between the concrete deck and steel girders was assumed to be 0.65 (Rabbat & Russell, 1985). Hard contact in the normal direction was used to prevent penetration. The ends of the diaphragms were tied to the web of the girders. Analyses with geometric nonlinearity were performed under the measured truckloads, approximated as 6-point loads. Self-weight was not included. Pin boundary conditions (i.e., free rotation in the transverse direction, fixed translation) was applied at the intersection of web and bottom flange for each girder line on one side of the bridge. Roller boundary conditions (i.e., free rotation in the transverse direction and free translation in longitudinal direction) was applied at the intersection of web and bottom flange for each girder line on the opposite side of the bridge. For the non-composite model, the translation of the concrete deck along one edge in the longitudinal and transverse direction was fixed to avoid numerical singularity. All models were simplified by neglecting the transverse slope of the deck and assuming the diaphragms were centered vertically along the girder webs.

The Category T damage was approximated using five parameters: rotation angle (α) between the web and the top flange, length of the damage (l_s), height of the web (d), the location of the start of the damage (D), and the location of the center or peak point of the damage (x) (Figure 4.1 and Table 4.1). The damaged shape of the bottom flange was approximated as a 5-degree polynomial, derived using (1) a start point (coordinates: 0,0,0), peak point (coordinates: x, $d\sin\alpha$, $d(1\text{-}\cos\text{-}\alpha)$, and end point (coordinates: l_s,0,0), and (2) the 1st order derivative at the start, peak, and end of the damage was required to be 0 to ensure smooth transition between the damaged and undamaged regions (Figure 4.1). A mesh for each damaged girder was generated in Rhinoceros (Robert McNeel & Associates, 2018; e.g., Figure 4.1c) and then imported into ABAQUS (2018) for numerical analysis. Specifically, nine evenly spaced points on the 5-degree polynomial function were imported in Rhinoceros and 5-degree interpolation was used to connect the points to generate a curve close to the theoretical polynomial function. The top flange was assumed to be not affected by the damage. The web was assumed to be perpendicular to the deformed bottom flange. Any local damage was ignored.

4.3 Asset 020-71-04052 (LaPorte District)

Asset 020-71-04052 (Figure 4.2 and Figure 4.3) is a three-span (50 ft. 6 in., 90 ft. 6 in., 50 ft. 6 in. spans) continuous composite bridge in South Bend, IN, built in 1966 and reconstructed in 1997. In 2016, 14 of the 22 girders were damaged near the East pier by a collision from an equipment hauler, with the heaviest damage incurred by the North exterior girder (Figure 4.4). Because of the vehicular collision, the lower flange was plastically deformed with a sweep of approximately 16 in. The bearing was also kicked out and retrofitted with a wedge.

Two girders were monitored (Figure 4.3): (1) severely damaged exterior girder (Location 1) and (2) less damaged symmetric exterior girder (Location 2). Location 1 is the location of the worst damage. Location 2 was selected as a symmetric location on a less damaged girder for comparison. Ideally, a symmetric undamaged girder would have been monitored. However, this was not possible, as some collision damage had occurred at Location 2. The behavior of the webs and bottom flanges were monitored. At Location 1, the bottom of the bottom flange and the North face of the web were monitored. At Location 2, the top of the bottom flange and the South face of the web were monitored.

Field work by the researchers was carried out over 3 days, facilitated by LaPorte District Maintenance Crews and INDOT Research & Development Staff (Figure 4.5). Load testing was performed to induce peak positive moment (tension in the bottom flange), peak negative moment (compression in the bottom flange), and peak shear in Location 1 and Location 2, with truck locations indicated in Table 4.2 (trucks were positioned 1 ft. away from the inner side of the concrete rail).

The FE model of Asset 020-71-04052 was simplified by ignoring the small skew angle. The damage of the North exterior girder was approximated based on field measurements (Table 4.1). The rotation angle (α) was determined based on a digital protractor measurement. The length of the damage (l_s) is equal to the distance between the 2nd and 5th diaphragms from the East. The location of the peak damage (x) is at the center of the splice plate. The 3rd and 4th diaphragms from the East of the damaged exterior girder are not modeled since they are disconnected from the girder. The length of the damage of the South exterior girder is 18 ft. (6 ft. in Northbound right Lane and 12 ft. in

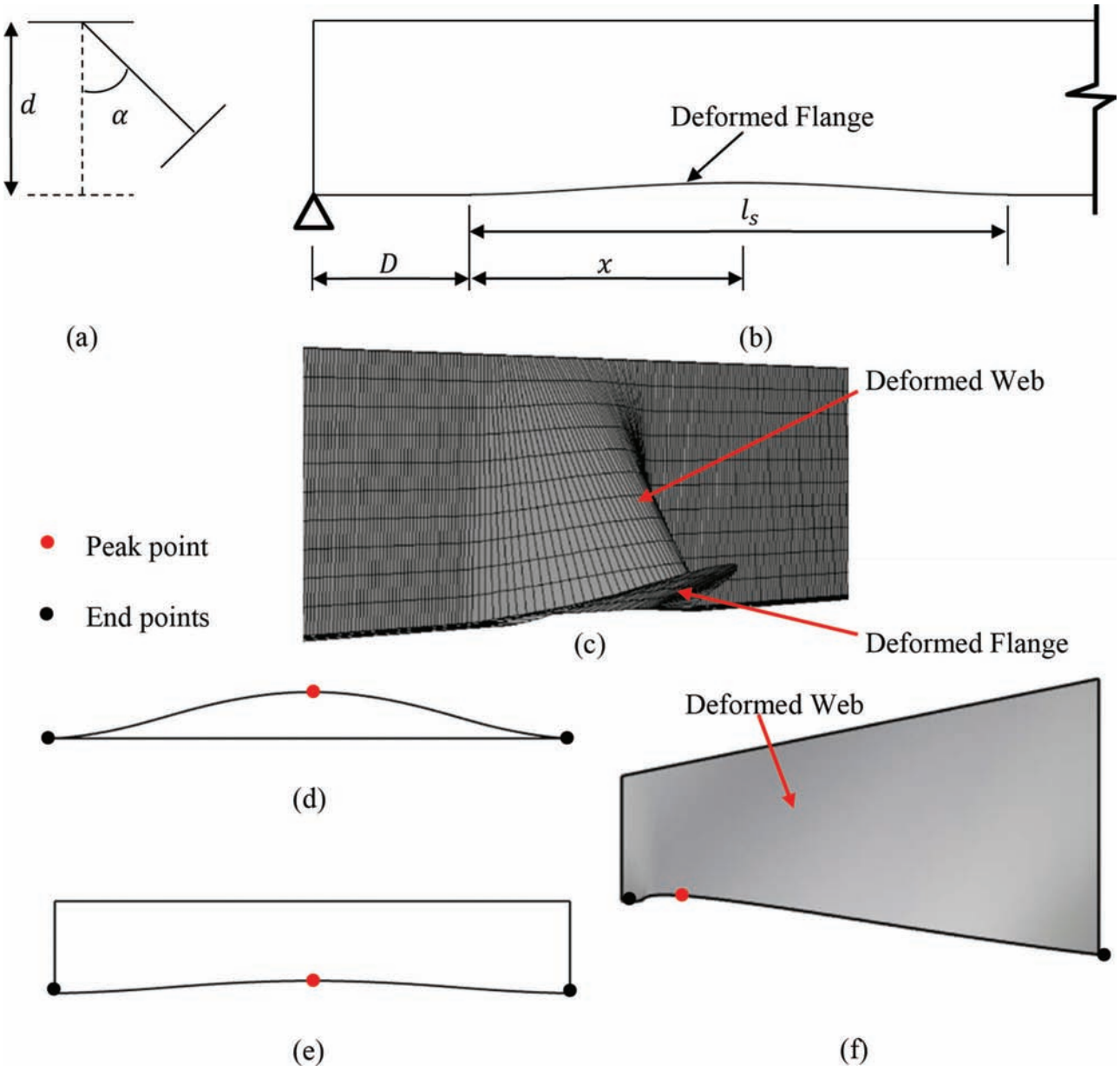

Figure 4.1 Parameters for approximating damage: (a) cross-section; (b) elevation; (c) 3D view, including mesh; (d) plan, (e) elevation, and (f) 3D view of the deformed shape of the center line of bottom flange.

TABLE 4.1
Parameters to model damaged girders for each bridge.

Asset No.	α (°)	l_s (in.)	x (in.)	D (in.)	d (in.)
020-71-04052 (N exterior)	30.0	780	430	370 (from East Pier)	32.2
020-71-04052 (S exterior)	10.8	216	106	693 (from East Pier)	32.2
030-02-04803 exterior	1.77	104	52.0	149 (from North Pier)	32.3
030-02-04803 interior	4.79	88.0	44.0	132 (from North Pier)	32.3
037-55-05265	14.0	325	180	840 (from West Pier)	34.8
(45)46-53-5993	19.9	355	142	1269 (from South Pier)	39.0

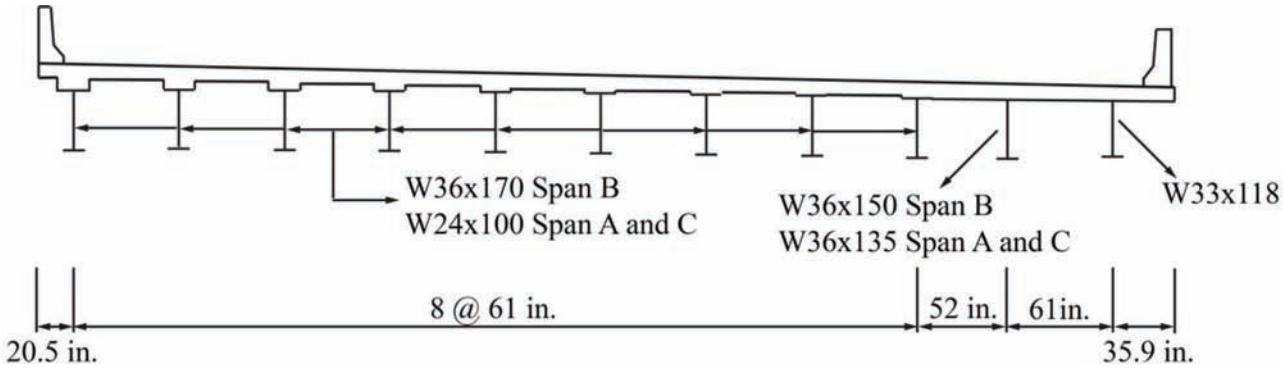

Figure 4.2 Cross-section of Asset 020-71-04052 (after reconstruction).

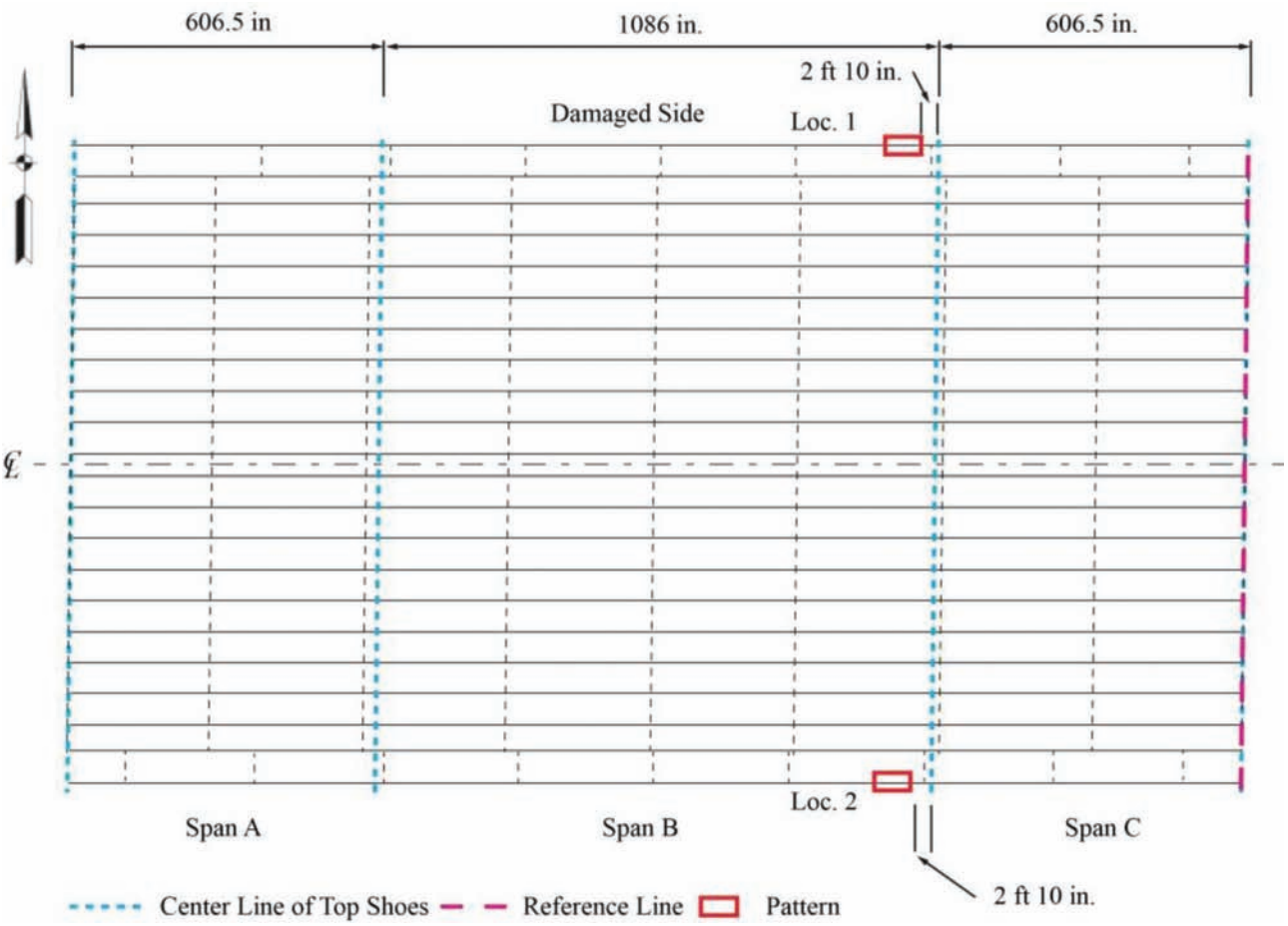

Figure 4.3 Framing plan and pattern locations for Asset 020-71-04052.

Northbound ramp) and the displacement is 6 in. according to the bridge inspection report from 2007.

Figure 4.6 and Table 4.3 show the DIC measured strains and the FE predictions under peak negative moment. For the damaged exterior girder (Location 1), two types of behavior between the damaged girder and the deck are considered: (1) in the center span and the East side span the girder and deck are composite (tied); (2) in the center span and the East side span the girder and deck are non-composite (untied). For both cases, the rest of the girders and the deck are composite. The latter case is studied to investigate if the damage affected the composite connection. Note that it is not expected that the strains in Location 1 match exactly the strains in Location 2 as the trucks could not be positioned in the same locations, but the values should be comparable. The strain would also be expected to differ as the bottom of the flange was monitored for

Location 1, while the top of the flange was monitored for Location 2. All later testing was performed on the bottom of the bottom flanges as the DIC cameras could be operated more easily from the ground.

Figure 4.6 and Table 4.3 show that strain in both girders is very small, demonstrating conservatism in design. The measured strain in the damaged girder (Location 1) is much smaller than the less damaged symmetric girder (Location 2). This suggests that load is being redistributed away from the damaged girders. Railing participation is likely an important consideration in this redistribution, as well as participation of adjacent girders. The FE prediction for the damaged girder using the tied model matches the measured data very well (full-field maps shown in Figure 4.6). The untied scenario results in smaller strains in the damaged girder. For the undamaged side, the FE prediction is less than the measurement. This is because the exterior girder on the undamaged side is also damaged and deformed inward. Figure 4.7 shows the FE strain distribution in the monitored region. Compared to the inner side, the monitored region has a lower average strain. This is because the strain distribution is very sensitive to the geometry of the damage. If more information is available on the less damaged side, better agreement could potentially be achieved between FE prediction and measured DIC results.

Figure 4.4 Damaged girder of Asset 020-71-04052.

Figure 4.5 Load testing for Location 2. (Photograph courtesy of Prince Baah.)

The measured strains under peak positive moment were very small (less than 0.01%) as the monitored locations were not in a position where high positive moment can be induced. The measured strains in the webs of Location 1 and Location 2 under peak shear were also very small (less than 0.01%). These low values of measured strain again indicate conservatism in design. Due to these low measured values, subsequent testing focused on the bottom of the bottom flanges.

4.4 Asset 030-02-04803 (Fort Wayne District)

Asset 030-02-04803 (Figure 4.8 and Figure 4.9) is a two-span (each 57 ft.) continuous non-composite bridge in Fort Wayne, IN, built in 1961 and reconstructed in 1985. The girders have been subjected to vehicular collision multiple times, with heat straightening occurring in 2004 and 2008. A tow truck pulling another vehicle caused the most recent 2008 collision. The truck hit the three westernmost beams. The 1st beam from West was bowed 4.5 in. to the West at a 10° angle. The 2nd beam from West had the most severe damage with 11.5 in. sweep and 30° rotation angle. The 3rd beam from West had a 9 in. sweep and 25° ration angle. All three beams had been heat straightened in the same year, but some damage remains, which was investigated (Figure 4.10).

Three girders were monitored (Figure 4.9): (1) severely damaged exterior girder (Location 1), (2) severely damaged interior girder (Location 2), and (3) less

TABLE 4.2
Truck weights, axle spacing, and wheel spacing for Asset 020-71-04052.

Loc.	Load case	Weights (k)/distance (in.)/transverse wheel spacing (in.)*					
1	Pos. Moment	9.24/1005/72	18.48/810/72	18.48/757/72	9.27/2158/72	18.54/1963/72	18.54/1910/72
	Neg. Moment	9.24/1150/72	18.48/955/72	18.48/902/72	9.27/1548/72	18.54/1353/72	18.54/1300/72
	Shear	9.24/932/72	18.48/737/72	18.48/684/72	9.27/1330/72	18.54/1135/72	18.54/1082/72
2	Pos. Moment	9.27/546/72	18.54/741/72	18.54/794/72	9.24/1773/72	18.48/1968/72	18.48/2021/72
	Neg. Moment	9.27/24/72	18.54/219/72	18.54/272/72	9.24/823/72	18.48/1018/72	18.48/1071/72
	Shear	9.27/506/72	18.54/701/72	18.54/754/72	9.24/932/72	18.48/1127/72	18.48/1180/72

*Distances measured from reference line in Figure 4.3.

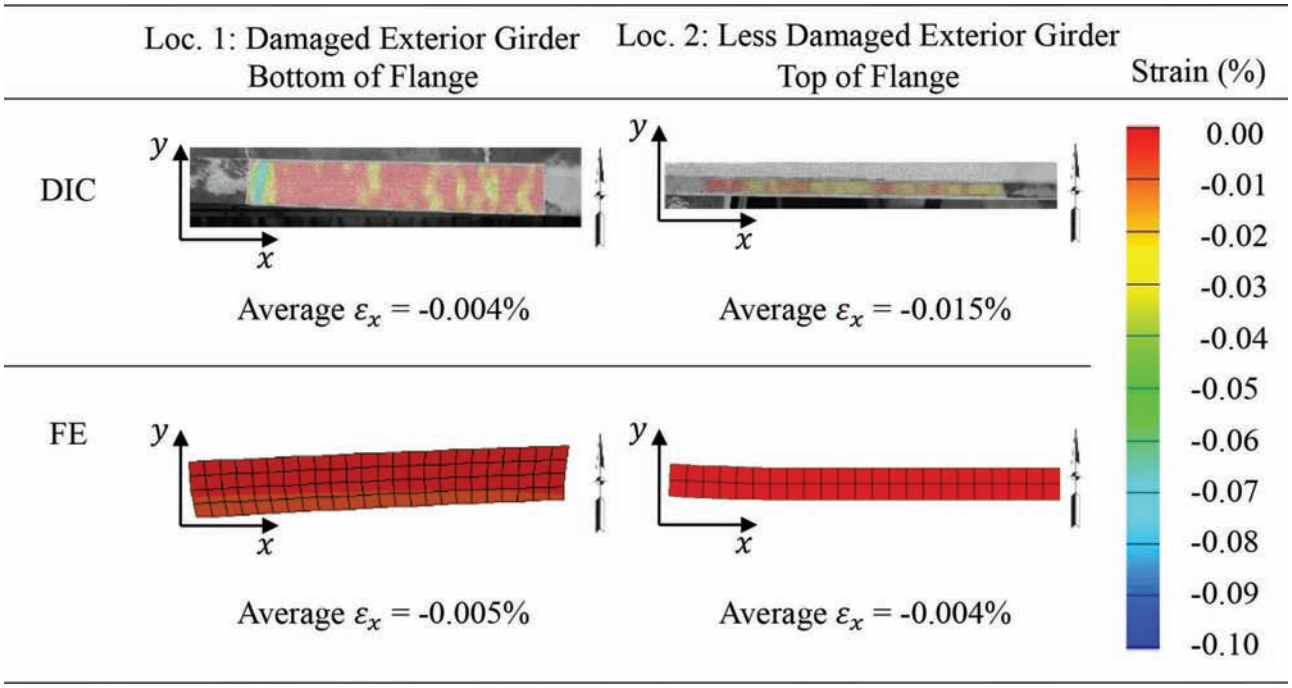

Figure 4.6 Measured and FE predictions (tied model) of strains in the bottom flanges of Asset 020-71-04052 under peak negative moment.

TABLE 4.3
Comparison of measured strain and FE prediction for Asset 020-71-04052.

Pattern location	DIC	FE
Loc. 1: Damaged Exterior Girder	-0.004%	-0.005% (tied) -0.002% (untied)
Loc. 2: Less Damaged Exterior Girder	-0.015%	-0.004%

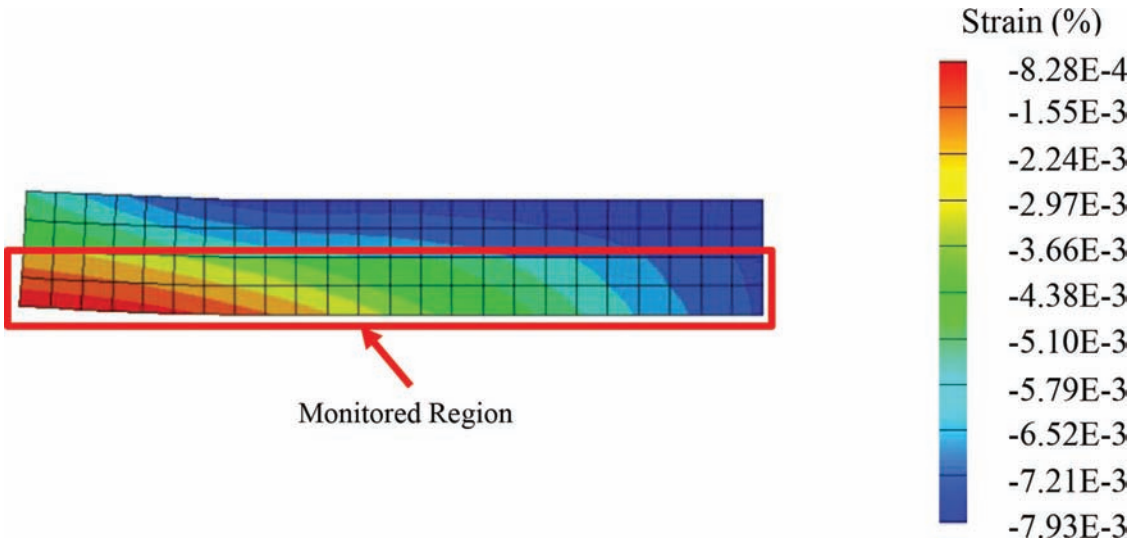

Figure 4.7 FE predictions of the strain distribution of Location 2 under peak negative moment.

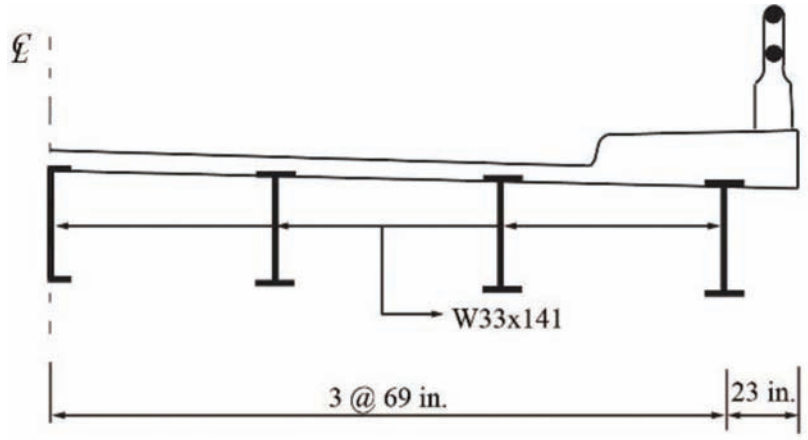

Figure 4.8 Cross-section of Asset 030-02-04803.

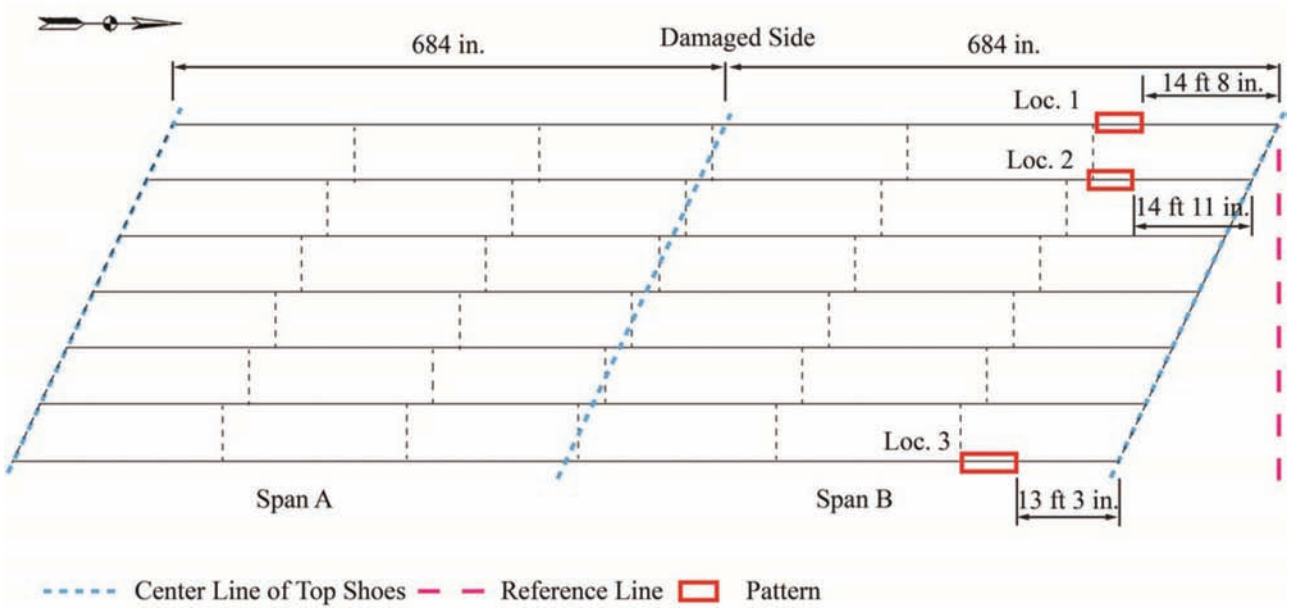

Figure 4.9 Framing plan and pattern locations for Asset 030-02-04803.

Figure 4.10 1st and 2nd damaged girder from West of Asset 030-02-04803.

damaged exterior girder (Location 3). Location 1 and Location 2 are selected as they were both severely damaged and load distribution between the two girders can be investigated. Location 3 is a symmetric location to Location 1 on a less damaged girder. The bottom of the bottom flanges for all three locations was monitored. Due to a crack in the web of Location 3, the web was also monitored.

Field work by the researchers was carried out over 2 days, facilitated by Fort Wayne District Maintenance Crews, Fort Wayne Bridge Inspectors, and INDOT Research & Development Staff (Figure 4.11). Load testing was performed to induce peak positive moment in the monitored regions, with truck locations indicated in Table 4.4. Only the peak positive moment loading condition was investigated, as it would not be possible to induce significant negative moment strains in the monitored regions. The truck dimensions and axle loads are provided in Table 4.4 (trucks were positioned about 2 in. away from the inner side of the concrete anchorage of the metal railing).

The FE model was built using the approach discussed earlier. The metal railing was not modeled. To investigate the effect of the concrete curb, the results from a model with concrete curb (modeled similarly to the concrete rail) is compared to one without. The bridge is non-composite and was modeled as untied along all girder lines. Since some composite behavior was still expected, a composite (tied) model was also investigated. The information on the damage was determined based on the DIC photographs (Figure 4.12). For the damaged exterior girder, the peak point of the damage is located at the center of the pattern. The damaged shape is assumed to be symmetrical and the peak point of the damage is centered along the pattern. The damage ends at the 1st diaphragm from the North. For the damaged interior girder, the damage is also assumed to be symmetrical and ends at the 1st diaphragm from the North. The peak point of damage is located at the North edge of the pattern.

Figure 4.13 and Table 4.5 show the measured DIC strains and FE predictions under peak positive moment. Overall, the strains are very small, again demonstrating conservatism in design. Since the measured strains are so small, the later studies focused on locations corresponding to where peak moment can be induced, as opposed to the location of the worst damage.

Like Asset 020-71-04052, the measured strain in the damaged exterior girder (Location 1) is much smaller than the less damaged symmetric girder (Location 3), suggesting load redistribution. Note that it is not expected that the strains in Location 1 and 3 match one another as the trucks could not be positioned in the same relative locations (since they were required to be facing with traffic), but the values should be comparable. This trend of damaged girders carrying less load is the same, despite Asset 030-02-04803 having a metal bridge rail with a small concrete curb (and therefore much less stiff rail) compared to the Asset 020-71-04052. The measured strain in the damaged interior girder (Location 2) is higher than that in the adjacent damaged exterior girder (Location 1). This indicates that the exterior girder is shedding load to the rail.

Figure 4.11 Load testing of Asset 030-02-04803.

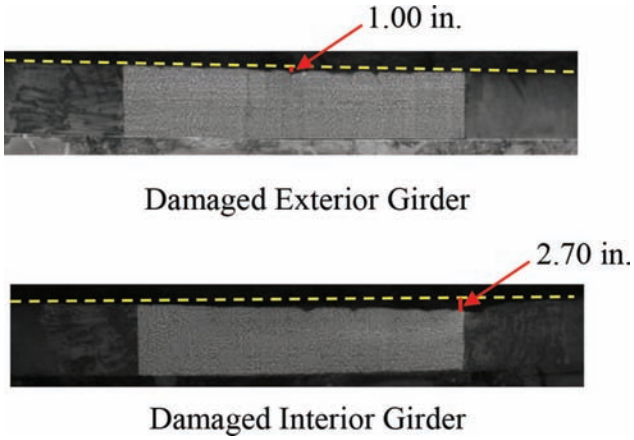

Figure 4.12 Displacement at the peak point of the damage of Asset 030-02-04803.

TABLE 4.4
Truck weights, axle spacing, and wheel spacing for Asset 030-02-04803.

Loc.	Load case	Weights (k)/distance (in.)/transverse wheel spacing (in.)*					
1	Pos. Moment	13.4/416/72	15.9/221/72	15.9/168/72	12.2/803/72	19.5/608/72	19.5/555/72
2	Pos. Moment	13.4/455/72	15.9/260/72	15.9/207/72	12.2/842/72	19.5/647/72	19.5/594/72
3	Pos. Moment	12.2/161/72	19.5/356/72	19.5/409/72	13.4/548/72	15.9/743/72	15.9/796/72

*Distances measured from reference line in Figure 4.9.

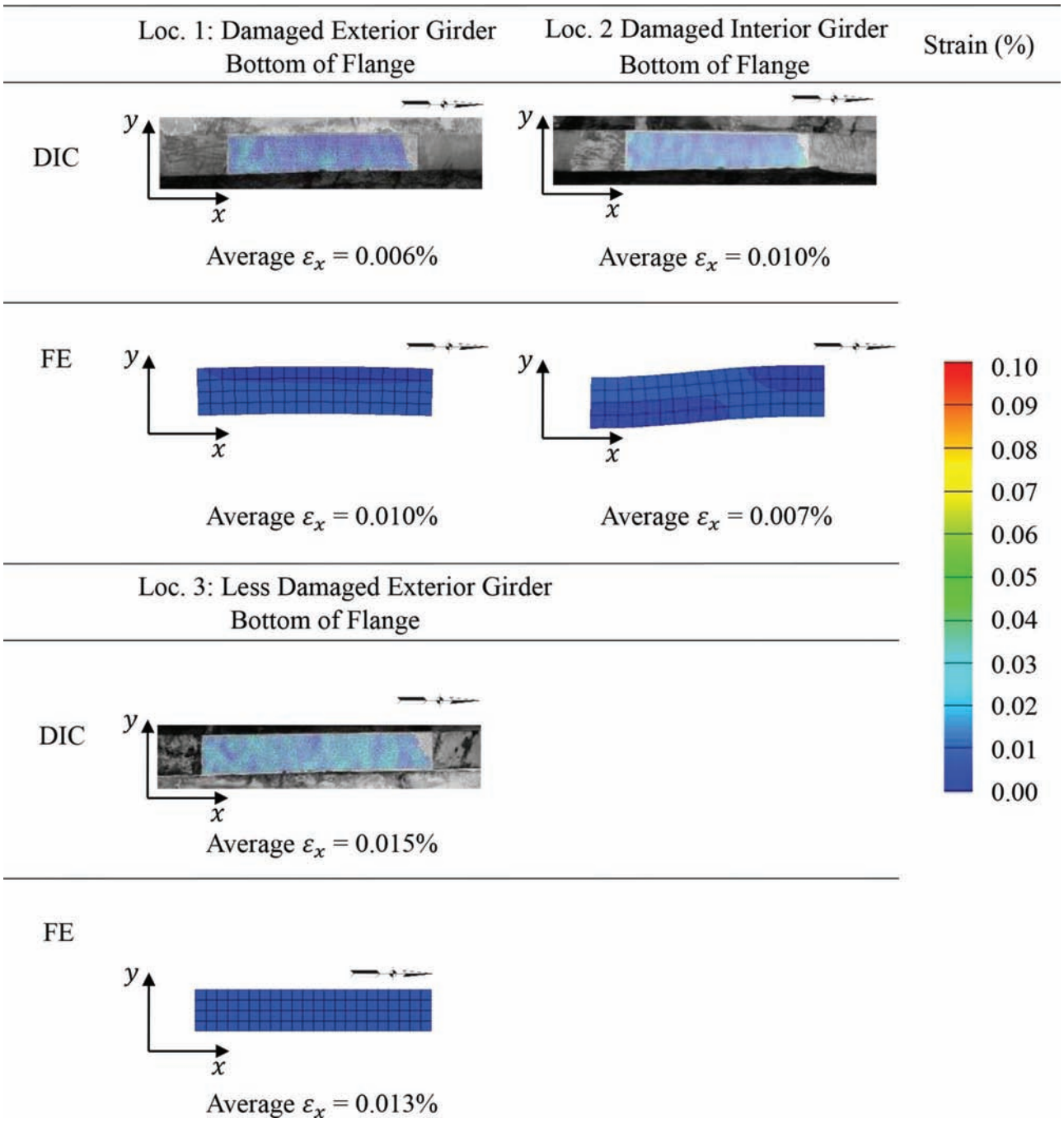

Figure 4.13 Measured and FE predictions (tied with curb) of strains in the bottom flanges in Asset 030-02-04803 under peak positive moment.

TABLE 4.5
Comparison of measured strain and FE prediction for Asset 030-02-04803.

Location	DIC	FE with curb	FE without curb
Loc. 1: Damaged Exterior Girder	0.006%	0.010% (tied) 0.011% (untied)	0.014% (tied) 0.018% (untied)
Loc. 2: Damaged Interior Girder	0.010%	0.007% (tied) 0.009% (untied)	0.009% (tied) 0.011% (untied)
Loc. 3: Undamaged Exterior Girder	0.015%	0.013% (tied) 0.018% (untied)	0.020% (tied) 0.026% (untied)
Undamaged Interior Girder	N/A	0.009% (tied) 0.010% (untied)	0.012% (tied) 0.014% (untied)

The participation of bridge rail will be an area for future study. Subsequent testing in this project will also focus on the adjacent interior girders to better understand the load redistribution.

The untied model results in a higher strain compared to the tied model, as would be expected. By adding the concrete curb, the strain drops significantly, which demonstrates the importance of even small concrete curbs. Overall, the tied FE model with the concrete curb most closely predicted the measured results.

Measured strains in the web of Location 3 under peak positive moment were negligible and no crack opening was observed.

4.5 Asset 037-55-05265 (Seymour District)

Asset 037-55-05265 (Figure 4.14 and Figure 4.15) is a two-span (70 ft. each) continuous composite bridge in Martinsville, IN, built in 1966 and reconstructed in 1990. All beams over SR 39 Northbound have some collision damage. The bridge has been hit several times; one collision was reported in 2013 and another one in 2015, which displaced the lower flange of the South exterior beam by 6 in. (Figure 4.16).

Four girders were monitored (Figure 4.15): (1) an undamaged exterior girder (Locations 1 and 2), (2) an undamaged interior girder adjacent to the undamaged exterior girder (Locations 3 and 4), (3) an undamaged interior girder adjacent to the damaged exterior girder (Locations 5 and 6), and (4) a damaged exterior girder (Locations 7, 8, and 9). Locations 1, 3, 5, and 7 were monitored as peak negative moment can be induced at these locations. Locations 2, 4, 6, and 8 were monitored as peak positive moment can be induced at these locations. Location 9 corresponds to the worst damage. The bottom of the bottom flanges were monitored.

Field work by the researchers was carried out over 2 days, facilitated by Seymour District Maintenance Crews, Seymour District Bridge Inspectors, and INDOT Research & Development Staff (Figure 4.17). Load testing was performed to induce peak negative moment and peak positive moment, with truck locations indicated in Table 4.6 (trucks were positioned 1 ft.

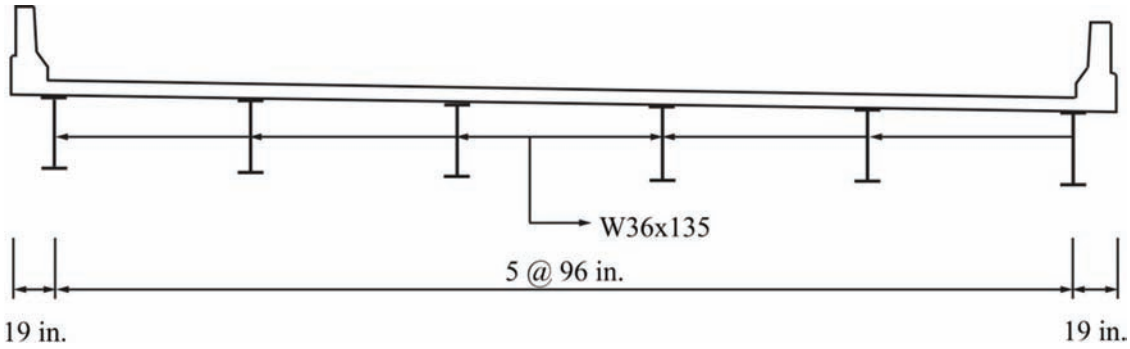

Figure 4.14 Cross-section of Asset 037-55-05265.

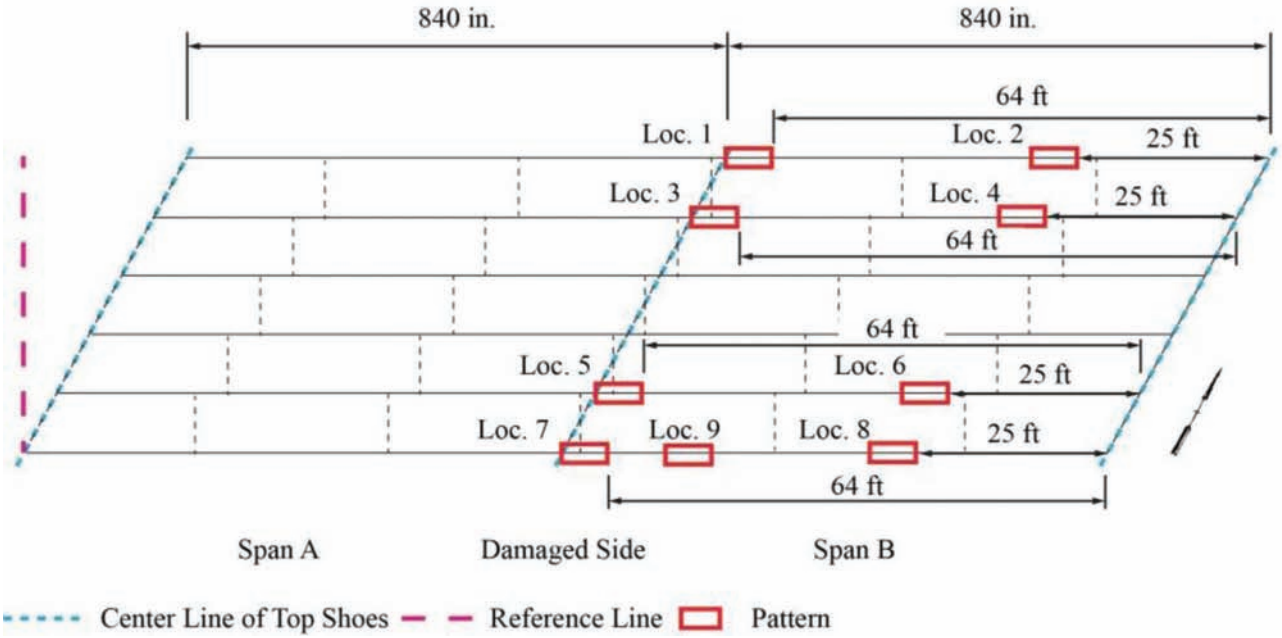

Figure 4.15 Framing plan and pattern locations for Asset 037-55-05265.

away from the inner side of the concrete rail). The truck positions are the same for the exterior girder and its adjacent interior girder.

For the FE model, the rotation angle (α) was determined based on field measurements using a digital protractor. The length of the damage (l_s) is equal to the distance between the center pier and the 4th diaphragm from the West. These parameters and the location of the peak of the damage (x) are shown in Table 4.1. According to the 2017 bridge inspection report, the girder was displaced 5 in. However, using the measured rotation angle, a displacement of 8.39 in. results. This was used in the FE model.

Figure 4.18 and Table 4.7 show the measured and predicted strains under peak positive moment. Again, the measured strains are small, indicating conservatism. The measured strains in the exterior girders (i.e., Locations 2 and 8) are comparable. However, the interior girder adjacent to the damaged girder (i.e., Location 6) carries more strain than any of the other girders. This demonstrates that the damaged girder is shedding its load to the adjacent girder. On the damaged side, different interactions between the concrete deck and the damaged girder were investigated numerically: (1) the damaged girder and the deck are acting compositely (tied); (2) the damaged girder and the deck are acting as non-composite between the 3rd and 5th diaphragm from the West and the coefficient of friction is 0.65 (united 1); (3) the damaged girder and the deck are acting as non-composite in the damaged span and the coefficient of friction is 0 (united 2); (4) the damaged girder and the deck are acting as non-composite in the damaged span and the coefficient of friction is 0.65 (untied 3). By removing the composite behavior over the entire damaged span and assuming no friction between the top flange and the deck (i.e., untied 2), the FE predictions most closely match the DIC measurements and are featured in Figure 4.18. This demonstrates that the shear connection between the girder and the deck may be damaged due to vehicular collision.

Additional studies removing the diaphragms between the damaged girder and the interior girder in the damaged span were also performed. The effect of removing the diaphragms was negligible.

The measured strains in all girders under peak negative moment were very small (less than 0.01%) as expected.

4.6 Asset (45)46-53-05993 (Seymour District)

Asset (45)46-53-05993 (Figure 4.19 and Figure 4.20) is two-span (96 ft. each) continuous non-composite bridge in Bloomington, IN, built in 1971 and reconstructed in 2003.

On August 21, 2018, a lift struck the East exterior girder in the North span. The girder was bent inward approximately 13 in. and the diaphragms punched through the girder in four locations including a hole near the splice plate at the approximate location of the impact (Figure 4.21). The Business Owner called the Principal Investigator that day to mobilize monitoring of this structure prior to any repairs. The researchers rapidly responded and performed monitoring—facilitated by

Figure 4.16 Damaged girder of Asset 037-55-05265.

Figure 4.17 Load testing for Asset 037-55-05265.

TABLE 4.6
Truck weights, axle spacing, and wheel spacing for Asset 037-55-05265.

Loc.	Load case	Weights (k)/distance (in.)/transverse wheel spacing (in.)*					
6/8	Pos. Moment	14.7/1584/85	25.6/1407/74	25.9/1354/74	16.3/1197/85	24.0/1029/74	23.8/974/74
5/7	Neg. Moment	14.7/1350/85	25.6/1173/74	25.9/1120/74	16.3/620/85	24.0/452/74	23.8/397/74
9	Pos. Moment	14.7/1635/85	25.6/1458/74	25.9/1405/74	16.3/1248/85	24.0/1080/74	23.8/1025/74
2/4	Pos. Moment	14.7/1835/85	25.6/1658/74	25.9/1605/74	16.3/1448/85	24.0/1280/74	23.8/120/74
1/3	Neg. Moment	14.7/1601/85	25.6/1424/74	25.9/1371/74	16.3/871/85	24.0/703/74	23.8/64/74

*Distances measured from reference line in Figure 4.15.

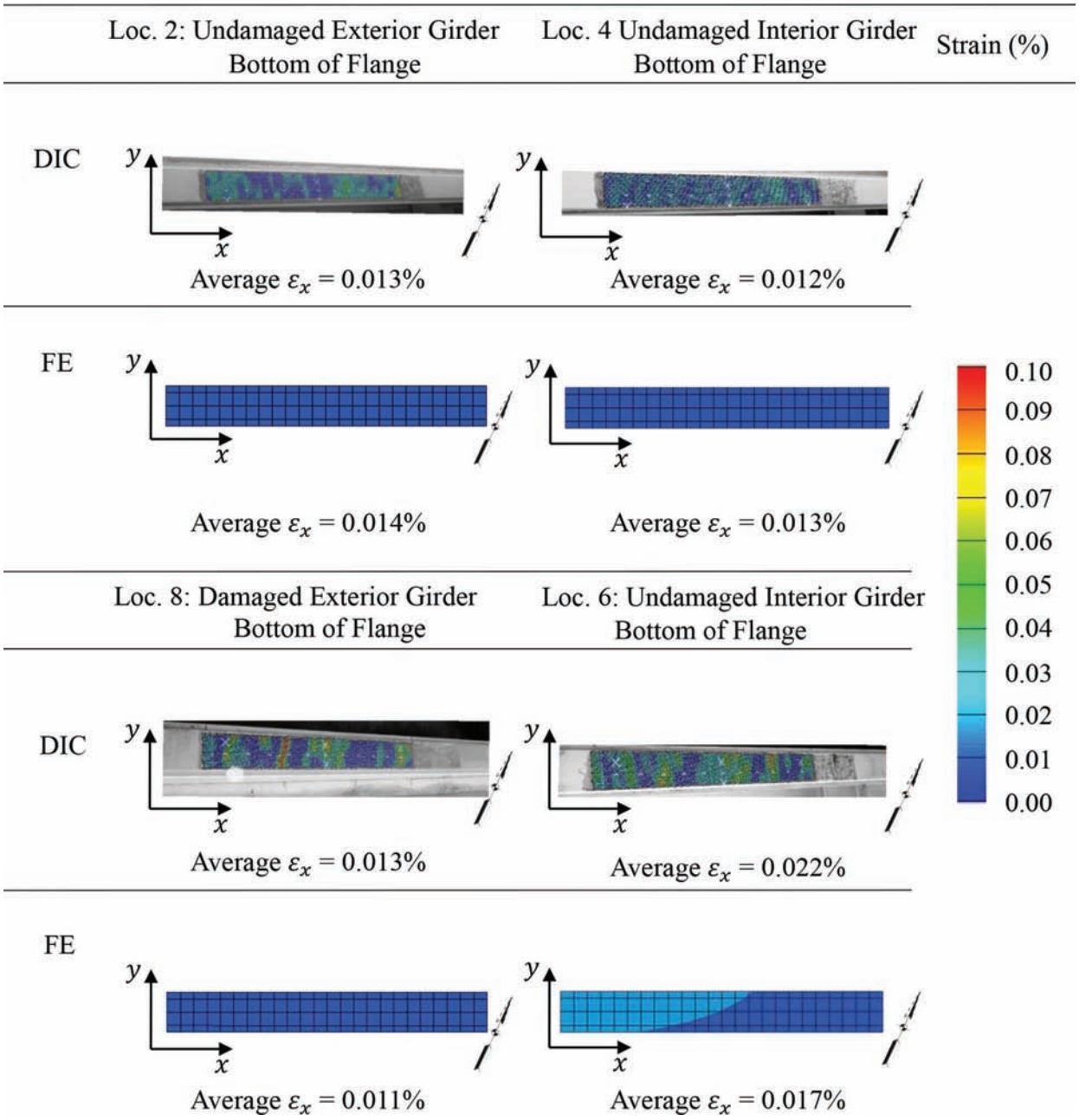

Figure 4.18 Measured and FE predictions (with damaged girder untied over the entire damaged span) of strains in the bottom flanges in Asset 037-55-05265 under peak positive moment.

TABLE 4.7
Comparison of measured strain and FE prediction for Asset 037-55-05265.

Location	DIC	FE
Loc. 2: Undamaged Exterior Girder	0.013%	0.014%
Loc. 4: Undamaged Interior Girder	0.012%	0.013%
Loc. 6: Undamaged Interior Girder	0.022%	0.013% (tied) 0.014% (untied 1) 0.017% (untied 2) 0.016% (untied 3)
Loc. 8: Damaged Exterior Girder	0.013%	0.015% (tied) 0.014% (untied 1) 0.011% (untied 2) 0.012% (untied 3)

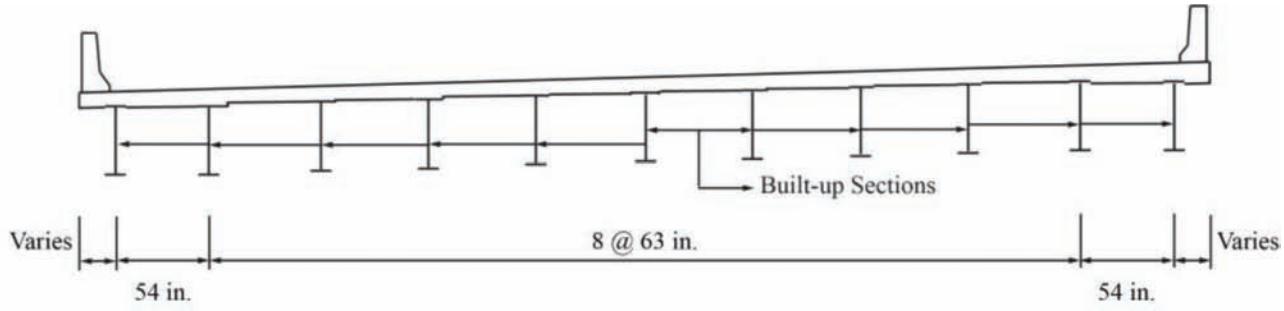

Figure 4.19 Cross-section of Asset (45)46-53-05993.

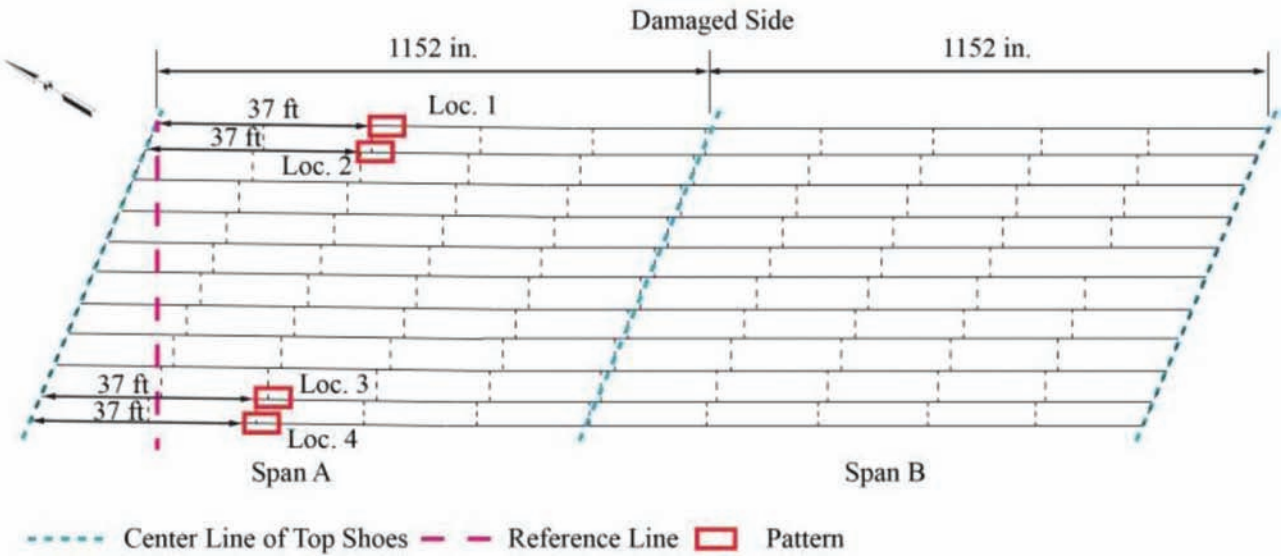

Figure 4.20 Framing plan and pattern locations for Asset (45)46-53-05993.

Figure 4.21 Damaged girder of Asset (45)46-53-05993.

Seymour District Maintenance Crews and Bridge Inspectors—on September 12, 2018, with both pattern application and monitoring occurring in the same day (Figure 4.22). While all other studies waited 48 hours between pattern application and monitoring to ensure cure time for the tape adhesive, this work was all performed in a single day. Tensile testing demonstrated that the adhesive provided sufficient bond immediately and therefore that monitoring could be performed immediately.

Figure 4.22 Load testing for Asset (45)46-53-05993.

Four girders were monitored (Figure 4.20): (1) a damaged exterior girder (Location 1), (2) an undamaged interior girder adjacent to the damaged girder (Location 2), (3) an undamaged interior girder (Location 3), and (4) an undamaged exterior girder (Location 4). Monitored regions were selected as peak positive moment

can be induced at these locations. The bottom of the bottom flanges were monitored.

Load testing was performed to induce peak positive moment, with truck locations and axle loads indicated in Table 4.8 (trucks were positioned 1 ft. away from the inner side of the concrete rail). During load tests, the trucks were all aligned in the same direction for a more direct comparison between the undamaged and damaged girders. The truck positions are the same for the exterior girder and its adjacent interior girder.

The North span was modeled as straight for simplicity. The survey data provided by GAI, Consultants, Inc. was used to determine the rotation angle (α), the location of the start of the damage (D), and the location of the center or peak point of the damage (x). The damage starts from 117 in. to the North of the center line of the center pier (survey data). The peak point of the damage is located 175.75 in. to the North of the start point and deformed 13.25 in. to the West (survey data). The damage ends at the 3rd diaphragm from the North (Table 4.1).

Figure 4.23 and Table 4.9 shows the measured and predicted strains under peak positive moment. Again, the strains are small, indicating conservatism. A notable

TABLE 4.8
Truck weights, axle spacing, and wheel spacing for Asset (45)46-53-05993.

Loc.	Load case	Weights (k)/distance (in.)/transverse wheel spacing (in.)*					
1/2	Pos. Moment	15.6/241/85	22.0/421/72	23.5/465/72	16.8/632/84	20.9/800/72	21.7/854/72
3/4	Pos. Moment	15.6/-20/85	22.0/160/72	23.5/204/72	16.8/371/84	20.9/539/72	21.7/593/72

*Distances measured from reference line in Figure 4.20.

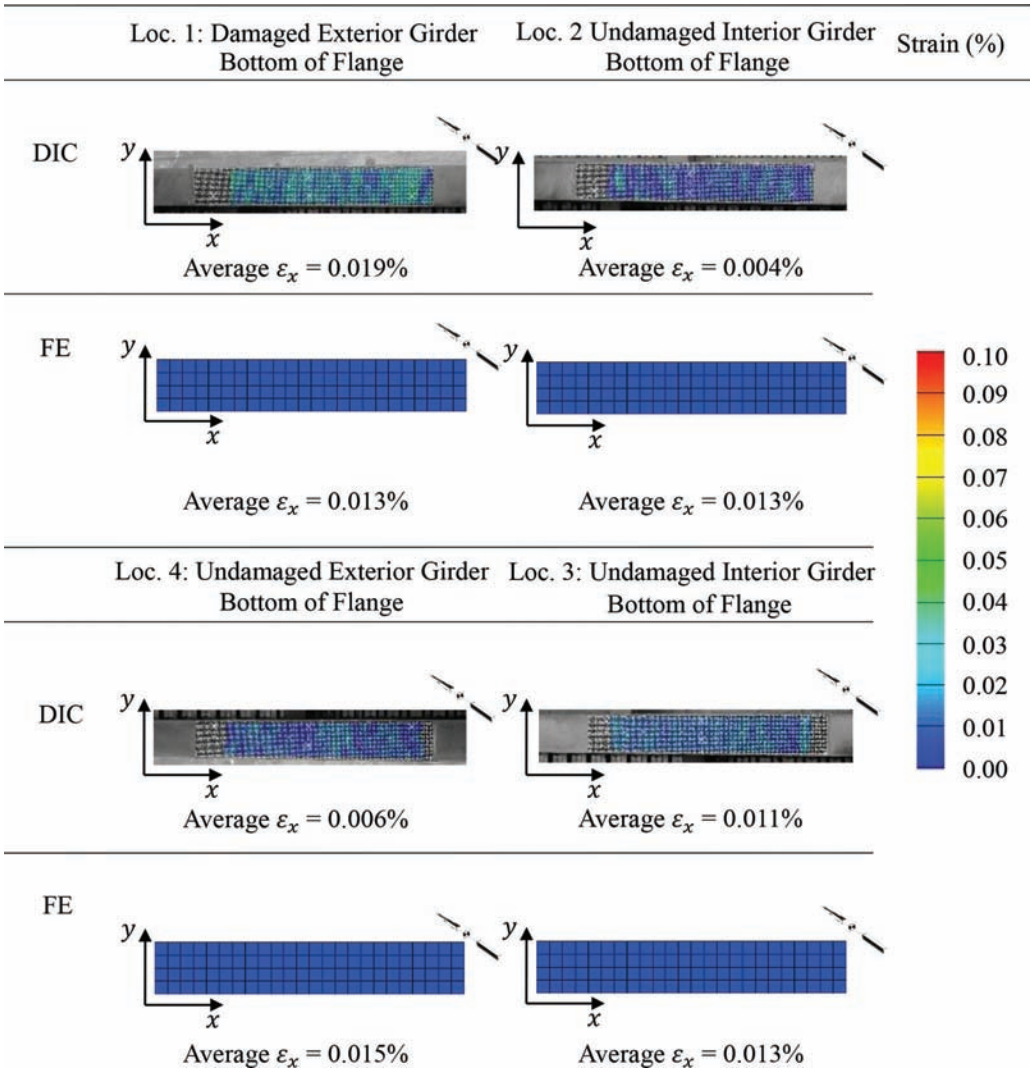

Figure 4.23 Measured and FE predictions (tied with cracks) of strains in the bottom flanges in Asset (45)46-53-05993 under peak positive moment.

TABLE 4.9
Comparison of measured strain and FE prediction for Asset (45)46-53-05993.

Location	DIC	FE
Loc. 1: Damaged Exterior Girder	0.019%	0.0129% (tied with 4th diaphragm) 0.013% (tied without 4th diaphragm) 0.005% (untied without 4th diaphragm) 0.013% (with hole) 0.0132% (with cracks)
Loc. 2: Undamaged Interior Girder	0.004%	0.0130% (tied with 4th diaphragm) 0.013% (tied without 4th diaphragm) 0.018% (untied without 4th diaphragm) 0.013% (with hole) 0.0133% (with cracks)
Loc. 3: Undamaged Interior Girder	0.011%	0.013%
Loc. 4: Undamaged Exterior Girder	0.006%	0.015%

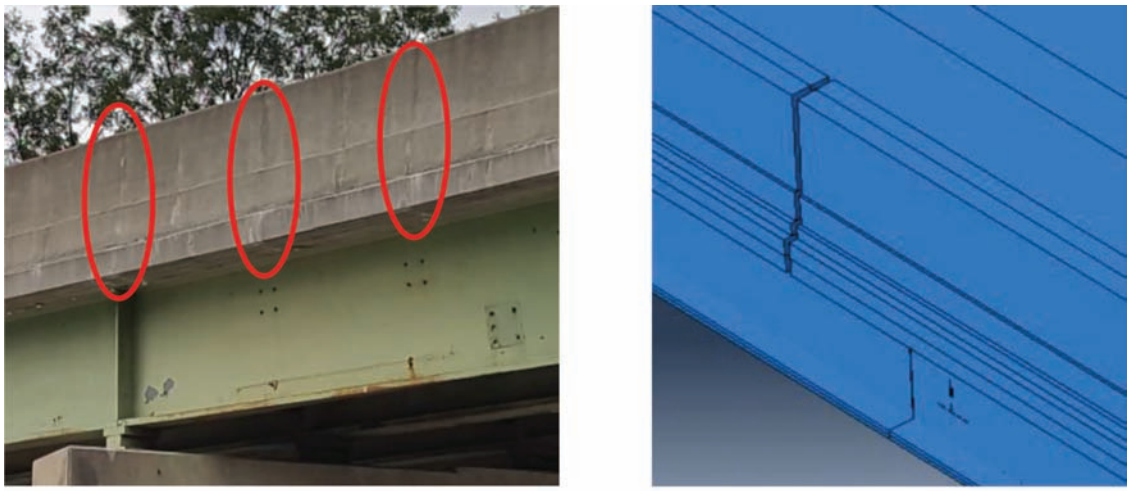

Figure 4.24 Cracks in the bridge and FE model.

difference in these measured results compared to the other bridges is that the exterior damaged girder (i.e., Location 1) carries higher strain than the other three girders. Varieties of numerical models were built to further investigate this behavior. The 4th diaphragm from the North, which is near the peak point of the damage, punched through the web. The effect of the hole (an ellipse with a major axis of 26 in. and a minor axis of 12 in.) was studied using FE model. The results show the effect of the hole on the monitored region is negligible. The effect of this diaphragm is investigated by comparing the results from one model with the 4th diaphragm from the North modeled and another without it. Removing this diaphragm had negligible effect on the strains. The interaction between the deck and the damaged girder in the damaged span is also investigated by assuming non-composite behavior (untied) and composite behavior (tied). By removing the composite behavior in the damaged span, the load redistributed away from the damaged girder to the adjacent undamaged girder. Further investigation of photographs of the bridge found that the bridge rail was severely cracked in the negative moment region (Figure 4.24). These cracks decrease the load carrying capacity and redistribute the positive moment. This effect was studied using the FE model by introducing a 1.5 in. wide gap in the railing and the deck. As shown in Table 4.9, the strains in the damaged girder and the adjacent undamaged interior girder increase. This demonstrates that cracked rail can increase the load carried by a damaged girder. Overall, the tied FE model with cracks on the damaged side gives results that are closest to the measured stain.

4.7 Summary

Table 4.10 summarizes the main research findings from each bridge studied.

TABLE 4.10
Bridge testing summary.

Asset no.	Research findings
020-71-04052	Strains are very small, indicating conservatism in design*
	The strain in the damaged girder is less than the symmetric undamaged girder, suggesting load redistribution to adjacent girders or bridge rail*
030-02-04803	Small concrete curb is participating in carrying load
037-55-05265	Shear connections between girder and deck may be damaged in a collision
(45)46-53-05993	Exterior damaged girder carries higher load
	Railing above damaged girder is severely cracked in negative moment region, causing redistribution of positive moment

*Indicates conclusion relevant to all bridges tested.

5. NUMERICAL PARAMETRIC INVESTIGATION

5.1 Approach

A parametric investigation, using the validated numerical modeling approach, was performed to understand the effect of varying shapes and locations of damage on load-deflection behavior. Finite element analyses were performed including nonlinear geometry and a nonlinear material model for the steel (based on the measured properties of the 0.5 in. thick steel in Figure 3.1 from Gerbo et al. [2016]). In models where the concrete deck is included, the concrete material is modeled elastically and strains remain below the tensile cracking limit. Self-weight was not considered.

Only Category T damage was investigated, as this was the type of damage observed in the four bridges studied. This was approximated using the same five variables as Chapter 4, with $x=l_s/2$. The investigation was first performed for a single girder and then for a three-span continuous bridge, with both studies modeled based on the dimensions of Asset 020-71-04052.

5.2 Single Girder Study

The study was performed for a W33 × 118 (d= 32.16 in.) simply supported girder with a span length S of 90 ft. 6 in. A pin boundary condition (i.e., free rotation in the transverse direction only, fixed translation) was applied at one end and a roller boundary condition (i.e., free rotation in the transverse direction only, free translation in the longitudinal direction only) was applied at the other. These boundary conditions were applied at a single node at the intersection of the web with the bottom flange. All nodes of the top flange were restrained in the transverse direction to simulate the restraint that that the deck would provide to resist lateral torsional buckling. An increasing uniformly distributed pressure load was applied to the top flange. Deflection at midspan was monitored. A total of 27 different damaged girders (Table 5.1) were investigated and compared with a straight (undamaged girder). The load-deflection behavior up to S/800 (service deflection limit according to AASHTO [2017]) was studied.

Generally, damage reduces the stiffness of the girder (Table 5.2, Figures 5.1, 5.2, and 5.3). The greater the

TABLE 5.1
Summary of parameters investigated in girder parametric study.

α (°)	l_s (in.)	D (in.)
10	60	0 (E)
20	120	S/4- l_s/2 (Q)
30	180	S/2- l_s/2 (C)

E: damage at end; Q: damage at quarter-span; C: damage at mid-span.

TABLE 5.2
Summary of elastic stiffness (% straight beam).

	α=10°	α=20°	α=30°
l_s=180 in. (C)	80.1	52.9	34.6
l_s=180 in. (Q)	92.4	76.3	60.5
l_s=180 in. (E)	98.0	93.8	88.3
l_s=120 in. (C)	82.2	56.2	36.5
l_s=120 in. (Q)	94.5	80.0	63.9
l_s=120 in. (E)	98.8	96.5	93.3
l_s=60 in. (C)	86.0	60.8	37.5
l_s=60 in. (Q)	96.2	84.6	67.0
l_s=60 in. (E)	99.5	98.5	97.2

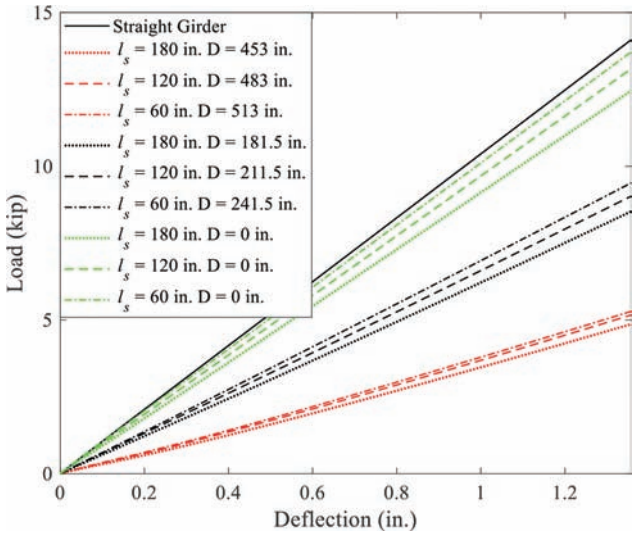

Figure 5.1 Load-deflection behavior for α=30°.

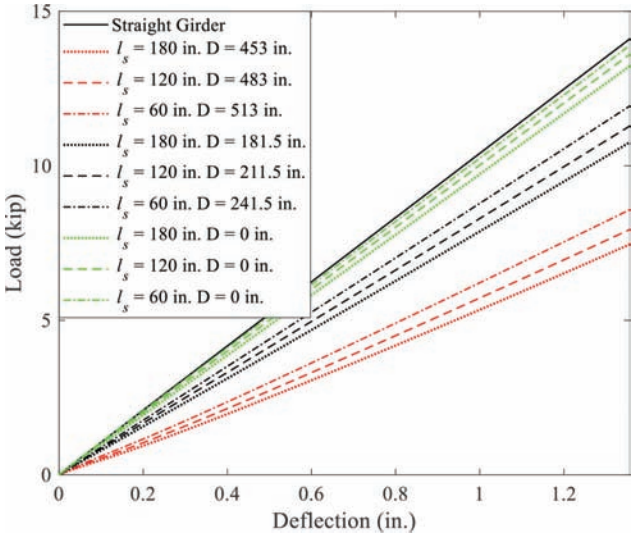

Figure 5.2 Load-deflection behavior for α=20°.

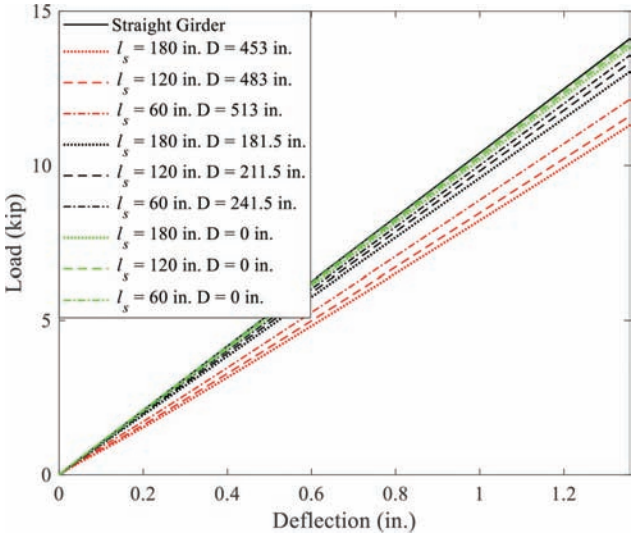

Figure 5.3 Load-deflection behavior for α=10°.

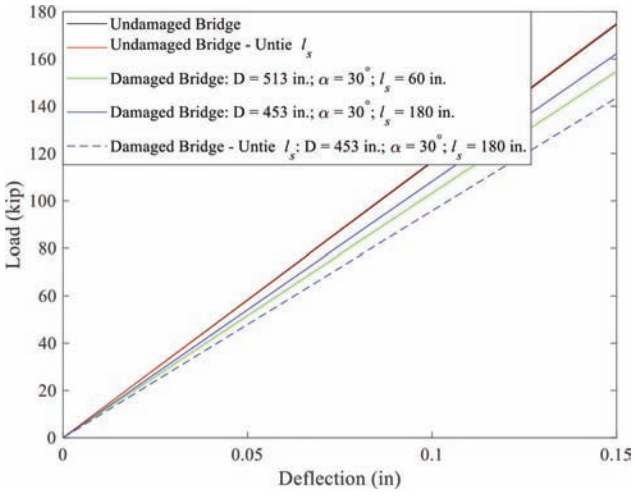

Figure 5.4 Load-deflection behavior of whole bridge.

rotation angle (α), the greater the reduction in the stiffness. As the damage moves from the edge of the girder to midspan, the effect of damage on the stiffness increases. Longer damaged lengths (l_s) also decrease the stiffness. The stiffness can drop up to 34.6% that of a straight beam when damage features a large rotation angle, long damage length, and midspan location.

5.3 Three-Span Continuous Bridge Study

For the three-span continuous bridge study, one exterior girder in the center span was modeled as damaged and the rest are undamaged. Based on results from the single girder study, two damage scenarios were considered: α=30°, l_s=180 in., D=S/2–l_s/2 and α=30°, l_s=60 in., D=S/2–l_s/2. Results were compared to a bridge with no damaged girders. The boundary conditions were the same as those in Chapter 4. An increasing uniformly distributed pressure load was applied over a 10 ft. transverse width, 1 ft. away from the inner side of the concrete railing, along the full bridge length. The deflection at the center of the damaged exterior girder was monitored.

The damaged girder reduces the stiffness of the entire bridge, compared to a bridge with no damaged girders (Figure 5.4). A shorter damaged length (l_s) decreases the stiffness of the bridge more than a longer length. This is in contrast to the findings of the single girder study. It can be attributed to continuity and load redistribution in the entire bridge model, where a longer damaged length is able to redistribute to adjacent girders more effectively than a more localized shorter length. Although damage can cause a significant drop in stiffness, in the single girder study (e.g., for α=30°, l_s=180 in., D=S/2–l_s/2, the damaged girder only had 34.6% of the stiffness of straight beam). This effect is mitigated in the entire bridge through redistribution to the concrete deck, concrete railing, and adjacent girders (for the same case, the stiffness of the bridge is 92.9% that of an undamaged bridge). The effect of removing the shear connection (or untying the connection between the girder and deck) was also investigated. This had a negligible effect on the undamaged bridge model, but resulted in a drop in stiffness from 92.9% for the undamaged bridge to 82.2% for α=30°, l_s=180 in., D=S/2–l_s/2.

5.4 Summary

This parametric investigation found that Category T damage decreases the stiffness of a girder, but that the magnitude of this effect is mitigated through continuity and redistribution in a continuous, multi-girder bridge system. As the damage moves from the end to the center of the girder, the effect of damage on the stiffness increases. A larger rotation angle decreases the stiffness. While a longer damaged length leads to greater decreases in stiffness for a single, isolated girder, a shorter damaged length has a more significant impact on the

stiffness of an entire bridge due to greater load redistribution potential for longer damaged lengths. Note that this study considered a limited range of parameters and the findings are limited to this range.

6. CONCLUSIONS

6.1 Summary of Research Findings

The main research findings are summarized as follows. These findings are limited to two- or three-span continuous multi-girder steel bridges for which an exterior girder has sustained Category T damage from a vehicular collision. Other categories of damage (e.g., highly localized damage or cracking) and other structural systems (e.g., girder floor beam systems) are excluded from these findings. These findings may be limited to the specific bridges monitored in this study with the specific type of damage observed.

1. DIC is a powerful monitoring technique, which can provide full-field measurements to understand system behavior and capture strain gradients.
2. Pressure activated adhesive tape (with a 10-year or more durability) has been qualified as a DIC pattern strategy to monitor strains in coated steel bridges. This approach can be implemented more rapidly than conventional pattern approaches (e.g., spray paint) to reduce the required time for lane closures, leading to cost savings and safety benefits for the traveling public. This has enabled DIC to be successfully used for field monitoring.
3. DIC, combined with finite element numerical modeling can provide a better understanding of bridge behavior.
4. The measured strains in all girders, subjected to quasi-static dump truck loads, are small (less than 0.022%, or approximately 6.4 ksi), demonstrating conservatism in design.
5. Loads are generally redistributed away from damaged girders to adjacent girders and rail. This is an area for future research.
6. Vehicular collision may damage the shear connectivity between the deck and the damaged girder in composite bridges.
7. Cracked or damaged railings may cause positive moment redistribution, resulting in higher strains in damaged girders.
8. Damage at the center of the span with a large rotation angle of the web results in the greatest loss of stiffness, compared to other locations and smaller rotation angles.
9. Load redistribution in multi-girder bridges and continuity generally reduce safety issues for Category T damage from vehicular collision. However, bridge inspectors must evaluate the potential for this load redistribution when evaluating bridges.

6.2 Expected Benefits, Deliverables, Implementation, and Cost Saving

These research findings have culminated in the *Recommendations for Bridge Inspectors for Evaluating Steel Girder Bridges Subjected to Vehicular Damage* document in the Appendix. Expected benefits from implementing these guidelines include: (1) bridge inspections following vehicular collision which are focused on identifying key factors that affect behavior (e.g., shear connectivity, rail cracking) and (2) prioritization of repair for bridges with specific damage profiles (e.g., damage in the center of a span with a large angle of deflection). This can result in INDOT cost savings as bridge inspections can be performed more quickly, bridges with the most severe damage (i.e., those with the greatest loss in stiffness) can be prioritized for repair, and unnecessary repairs could potentially be avoided.

The implementation plan for this research includes:

1. The *Recommendations for Bridge Inspectors for Evaluating Steel Girder Bridges Subjected to Vehicular Damage* document will be made available on the INDOT website and will be considered in the upcoming rewrite of the *Indiana Bridge Inspection Manual*.
2. Research results and these recommendations will be presented at the INDOT Bridge Inspector Workshop on February 13, 2019 (presentation will be available online for bridge inspectors' reference for one year), the 2019 Purdue Road School, and the INDOT/Joint Transportation Research Program Poster Session on February 13, 2019.
3. The Final Report will be posted on the Purdue e-Pubs website and will be freely available publicly.
4. To further investigate rail participation, a new project, *Evaluating Reserve Strength of Girder Bridges due to Bridge Rail Load Shedding* (SPR-4311), has been awarded.

Deliverables include the following.

PhD Dissertation

Wang, Y. *Monitoring the behavior of bridges using digital image correlation.* PhD dissertation to be submitted.

Peer-Reviewed Journal Publications

Wang, Y., Tumbeva, M. D., Thrall, A. P., & Zoli, T. P. Pressure activated adhesive tape pattern for monitoring the structural condition of steel bridges via digital image correlation. *Structural Control and Health Monitoring*. Submitted September 2018.

Wang, Y., & Thrall, A. P. *Behavior of steel girder bridges subjected to vehicular collision*. Manuscript in preparation.

Presentations

Wang, Y., & Thrall, A. P. (2019). Behavior of bridges subjected to vehicular collision. *Purdue Road School*, West Lafayette, IN, March 4–7, 2019.

Wang, Y., & Thrall, A. P. (2019). Assessment of bridges subjected to vehicular collision. *Indiana Department of Transportation Bridge Inspector Workshop*, Indianapolis, IN, February 13, 2019.

Wang, Y., & Thrall, A. P. (2018). Monitoring bridges by digital image correlation. *North Central States Consortium 2018*, Grand Rapids, MI, October 23–24, 2018.

Wang, Y., & Thrall, A. P. (2018). Assessment of bridges subjected to vehicular collision. *Indiana Department of Transportation Bridge Inspector Workshop*, Indianapolis, IN, February 6, 2018.

Wang, Y., Thrall, A. P., & Zoli, T. P. (2018). Assessment of bridges subjected to vehicular collision. *Joint Transportation Research Program—Indiana Department of Transportation Poster Session*, Indianapolis, IN, February 5, 2018; *Purdue Road School*, West Lafayette, IN, March 6, 2018.

Wang, Y., Thrall, A. P., & Zoli, T. P. (2017). Assessment of bridges subjected to vehicular impact. *Joint Transportation Research Program—Indiana Department of Transportation Poster Session*, Indianapolis, IN, February 15, 2017.

Website

Assessment of bridges subjected to vehicular collision. (2018).https://athrall.nd.edu/vehicular_collision.html

6.3 Future Studies and Further Uses of Research Findings

Results from this project indicate that bridge rails participate in carrying live load. To further investigate rail participation, a new INDOT project has been awarded: *Evaluating Reserve Strength of Girder Bridges due to Bridge Rail Load Shedding* (SPR-4311). This project (beginning January 2019) will investigate the participation of bridge rails through (1) performing non-destructive field testing, (2) developing validated numerical models, and (3) performing parametric numerical investigations to extend results to other loadings and bridge geometries.

The developed patterning strategy has been implemented to (1) monitor the repair of the Delaware River Bridge (Wang, Thrall, & Zoli, 2018) and (2) measure the erection-induced strains of the Governor Mario M. Cuomo Bridge (Wang, Thrall, & Zoli, 2019).

ACKNOWLEDGMENTS

The Joint Transportation Research Program administered by the Indiana Department of Transportation (INDOT) and Purdue University supported this work. The support of Business Owner Randy Strain, Project Advisor Prince Baah, and Study Advisory Committee Members Tim Wells, Mark Pittman, and Nathaniel Pfeiffer is gratefully acknowledged. The authors are grateful to INDOT maintenance crews of LaPorte, Fort Wayne, and Seymour Districts, as well as Anthony Johnson, for their support of the field monitoring. Graduate students Mirela Tumbeva, Evan Gerbo, and Anne O'Donnell are acknowledged for their contributions. The authors appreciate the guidance provided by Ted Zoli of HNTB Corporation and 3M. The contents of this report reflect the views of the authors, who are responsible for the facts and accuracy of the data presented herein, and do not necessarily reflect the official views or policies of the sponsoring organizations. These contents do not constitute a standard, specification, or regulation.

REFERENCES

AASHTO. (2017). *AASHTO LRFD bridge design specifications* (8th ed.). Washington, DC: American Association of State Highway and Transportation Officials.

ABAQUS. (2014). *ABAQUS/standard analysis user's manual*. Waltham, MA: Dassault Systèmes.

ABAQUS. (2018). *ABAQUS/standard analysis user's manual*. Waltham, MA: Dassault Systèmes.

ARAMIS. (2013). *ARAMIS user manual*. Braunschweig, Germany: GOM.

ARAMIS. (2017). *ARAMIS user manual*. Braunschweig, Germany: GOM.

ASTM. (2010a). *Standard test method for Poisson's ratio at room temperature* (ASTM E132-04). West Conshohocken, PA: ASTM International. https://doi.org/10.1520/E0132-17

ASTM. (2010b). *Standard test method for Young's modulus, tangent modulus, and chord modulus* (ASTM E111-04). West Conshohocken, PA: ASTM International. https://doi.org/10.1520/E0111-04R10

ASTM. (2014a). *Standard specification for general requirements for rolled structural steel bars, plates, shapes, and sheet piling* (ASTM A6/A6 M-14). West Conshohocken, PA: ASTM International. https://doi.org/10.1520/A0006_A0006M-17A

ASTM. (2014b). *Standard test methods and definitions for mechanical testing of steel products* (ASTM A370-14). West Conshohocken, PA: ASTM International. https://doi.org/10.1520/A0370-17A

Avent, R. R. (1989). Heat-straightening of steel: Fact and fable. *Journal of Structural Engineering*, *115*(11), 2773–2793. https://doi.org/10.1061/(ASCE)0733-9445(1989)115:11(2773)

Avent, R. R. (2015). *Guide for heat-straightening of damaged steel bridge members* (Report No. FHWA-IF-08-999). Washington, DC: Federal Highway Administration Office of Acquisition Management. Retrieved https://www.fhwa.dot.gov/bridge/steel/heat_guide.pdf

Avent, R. R., Robinson, P. F., Madan, A., & Shenoy, S. (1992). *Development of engineering design procedures for heat-straightening repair of damaged structural steel in bridges* (Report No. FHWA/LA-92/251). Baton Rouge, LA: Louisiana Transportation Research Center. Retrieved from https://www.ltrc.lsu.edu/pdf/2013/fr_251.pdf

Baah, P. (2014). *Cracking behavior of structural slab bridge decks* (Doctoral dissertation). Akron, OH: University of Akron. https://etd.ohiolink.edu/pg_10?0::NO:10:P10_ACCESSION_NUM:akron1417539467#abstract-files

Baldoni, J., Lionello, G., Zama, F., & Cristofolini, L. (2016). Comparison of different filtering strategies to reduce noise in strain measurement with digital image correlation. *Journal of Strain Analysis for Engineering Design*, *51*(6), 416–430. https://doi.org/10.1177/0309324716646690

Bell, E. S., Gaylord, D., Goudreau, A., & White, D. (2015). *Instrumentation, digital image correlation, and modeling to monitor bridge behavior and condition assessment* (Report No. FHWA-NH-RD-15680L). Concord, NH: New Hampshire Department of Transportation. Retrieved from

https://www.nh.gov/dot/org/projectdevelopment/materials/research/projects/documents/15680L-FINALREPORT.pdf

Bell, E. S., Peddle, J. T., & Goudreau, A. (2012). Bridge condition assessment using digital image correlation and structural modeling. In *Bridge maintenance, safety, management, resilience and sustainability: Proceedings of the Sixth International IABMAS Conference* (pp. 330–337). Boca Raton, FL: CRC Press.

Busca, G., Cigada, A., Mazzoleni, P., & Zappa. E. (2014). Vibration monitoring of multiple bridge points by means of a unique vision-based measuring system. *Experimental Mechanics*, *54*(2), 255–271. https://doi.org/10.1007/s11340-013-9784-8

Chiang, C.-H., Shih, M.-H., Chen, W., & Yu C.-P. (2011). Displacement measurements of highway bridges using digital image correlation methods. In *Proc. SPIE 8321: Seventh International Symposium on Precision Engineering Measurements and Instrumentation*, 83211G. https://doi.org/10.1117/12.904303

Connor, R. J., Urban, M. J., & Kaufmann, E. J. (2008). *Heat-straightening repair of damaged steel bridge girders: Fatigue and fracture performance* (National Cooperative Highway Research Program Report 604). Washington, DC: Transportation Research Board. https://doi.org/10.17226/23087

El-Hajjar, R. F., & Petersen, D. R. (2011). Adhesive polyvinyl chloride coatings for quantitative strain measurement in composite materials. *Composites Part B: Engineering*, *42*(7), 1929–1936. https://doi.org/10.1016/j.compositesb.2011.05.041

Gerbo, E. J., Thrall, A. P., Smith, B. J., & Zoli, T. P. (2016). Full-field measurement of residual strains in cold bent steel plates. *Journal of Constructional Steel Research*, *127*, 187–203. https://doi.org/10.1016/j.jcsr.2016.07.026

Huebschman, C. R., Garcia, C., Bullock, D. M., & Abraham, D. M., (2003). *Construction work zone safety* (Joint Transportation Research Program Publication No. FHWA/IN/JTRP-2002/34). West Lafayette, IN: Purdue University. https://doi.org/10.5703/1288284313166

Hoag, A. J., Hoult, N. A., Take, W. A., & Le, H. (2015). Monitoring of rail bridge displacements using digital image correlation. In *Proceedings of the 10th International Workshop on Structural Health Monitoring*, *2*, 399–406. https://doi.org/10.12783/SHM2015/52

Kim, S.-W., & Kim, N.-S. (2013). Dynamic characteristics of suspension bridge hanger cables using digital image processing. *NDT & E International*, *59*, 25–33. https://doi.org/10.1016/j.ndteint.2013.05.002

Lackowski, M., & Varma, A. (2007). *Synthesis study: Heat treatment and its effects on rehabilitating steel bridges in Indiana* (Joint Transportation Research Program Publication No. FHWA/IN/JTRP-2007/03). West Lafayette, IN: Purdue University. https://doi.org/10.5703/1288284313371

Langfield, A. (2013, August 5). *Wayward trucks smash into Indianapolis bridges 400 times. CNBC.* Retrieved from http://www.cnbc.com/id/100928291

Nonis, C., Niezrecki, C., Yu, T. Y., Ahmed, S., Su, C. F., & Schmidt, T. (2013). Structural health monitoring of bridges using digital image correlation. In *Proc. SPIE 8695: Health Monitoring of Structural and Biological Systems 2013, 869507*. 2013, 869507-1–869507-13. https://doi.org/10.1117/12.2009647

Peddle, J., Goudreau, A., Carlson, E., & Santini-Bell, E. (2011). Bridge displacement measurement through digital image correlation. *Bridge Structures*, *7*(4), 165–173. https://doi.org/10.3233/BRS-2011-031

Rabbat, B. G., & Russell, H. G. (1985). Friction coefficient of steel on concrete or grout. *Journal of Structural Engineering*, *113*(3), 505–515. https://doi.org/10.1061/(ASCE)0733-9445(1985)111:3(505)

Robert McNeel & Associates. (2018). Rhinoceros [Computer application]. Seattle, WA: Robert McNeel & Associates.

Schmidt, T., Tyson, J., & Galanulis, K. (2003). Full-field dynamic displacement and strain measurement using advanced 3D image correlation photogrammetry: Part I. *Experimental Techniques*, *27*(3), 47–50. https://doi.org/10.1111/j.1747-1567.2003.tb00115.x

Sutton, M. A., Orteu, J-J., & Schreier, H. (2009). *Image correlation for shape, motion and deformation measurements: Basic concepts, theory and applications*. New York, NY: Springer. Retrieved from https://doi.org/10.1007/978-0-387-78747-3

Varma, A. H., & Kowalkowski, K. J. (2004). *Effects of multiple damage-heat straightening repair on the fundamental properties of bridge steels* (Publication RC-1456). Lansing, MI: Michigan Department of Transportation. Retrieved from https://www.michigan.gov/documents/mdot_RC-1456A_Part_1_114188_7.pdf

Varma, A. H., & Sohn, Y. (2013). *Effects of realistic heat straightening repair on the properties and serviceability of damaged steel beam bridges* (Joint Transportation Research Program, Publication No. FHWA/IN/JTRP-2013/03). West Lafayette, IN: Indiana Department of Transportation and Purdue University. https://doi.org/10.5703/1288284315184

Wang, Y., Thrall, A. P., & Zoli, T. P. (2018). Delaware River Bridge fracture: Repair strategy and monitoring by digital image correlation. In *Proceedings of the World Steel Bridge Symposium*. Retrieved from https://www.aisc.org/globalassets/nsba/conference-proceedings/2018/2018-wsbs-final-paper---thrall.pdf

Wang, Y., Thrall, A. P., & Zoli, T. P. (2019). *Monitoring the Governor Mario M. Cuomo Bridge by digital image correlation*. Paper presented at the 2019 ASCE Structures Congress. Abstract retrieved from https://eventscribe.com/2019/STCONG19/fsPopup.asp?efp=RkdUVFpLWUs0MDQ3&PresentationID=455454&rnd=0.4081898&mode=presinfo

Winkler, J., Hendy, C. R., & Waterfall, P. (2015). Improved structural health monitoring strategies for better management of civil infrastructure systems. In *Multi-span large bridges: Proceedings of the International Conference on Multi-Span Large Bridges* (pp. 855–862). London, UK: Taylor & Francis.

Yoneyama, S., Kitagawa, A., Iwata, S., Tani, K., & Kikuta, H. (2007). Bridge deflection measurement using digital image correlation. *Experimental Techniques*, *31*(1), 34–40. https://doi.org/10.1111/j.1747-1567.2006.00132.x

APPENDIX

RECOMMENDATIONS FOR BRIDGE INSPECTORS FOR EVALUATING STEEL GIRDER BRIDGES SUBJECTED TO VEHICULAR DAMAGE

Bridge inspectors can use the following recommendations to evaluate two- or three-span continuous multi-girder steel bridges for which an exterior girder has sustained Category T damage, i.e., torsion about the longitudinal direction (as shown for example in Figure A.1; FHWA [2015]), from a vehicular collision. Other categories of damage (e.g., highly localized damage or cracking) and other structural systems (e.g., girder floor beam systems) are excluded from these recommendations and should be evaluated separately.

1. Bridges should always be inspected after a vehicular collision.
2. Generally, load redistribution in multi-girder bridges and continuity reduce safety issues for Category T damage from vehicular collision. Bridge inspectors must evaluate this load redistribution potential for each case. The measure of redundancy (for example as it relates to number of girders, spacing of girders) to provide this load redistribution is an area for future research.
3. During inspection of composite bridges, special attention should be paid to the shear connection between the girder and deck as this can be damaged during collision and result in higher live load strains in the steel girders.
4. Category T damage in the center of a span with a large angle of deflection of the web, results in the most severe loss of stiffness. Bridges with this type of damage should be prioritized for repair.
5. Girders adjacent to damaged girders may carry live load that is being redistributed away from the damaged girder. While the expected strain in these adjacent girders is still small, they should be inspected for increased deflections as an indication of carrying higher loads.
6. Bridge rails participate in carrying live load. This is an area for future research, but repairs should be implemented to reduce reliance on rail participation.
7. Bridges with open rails, severely cracked or damaged rails, and/or less redundancy (related to number or spacing of girders) require a more detailed evaluation.
8. Inspectors should take into account prior heat straightening of damaged girders and its effect on the material properties of the steel when evaluating a girder.

These recommendations are based on measured data and numerical finite element model predictions from SPR-4119: *Assessment of Bridges Subjected to Vehicular Collision*. These recommendations may be limited to the specific bridges monitored in this study with the specific type of damage observed (Figure A.1).

APPENDIX REFERENCE

FHWA (2015). *Guide for heat-straightening of damaged steel bridge members*. Retrieved from http://www.fhwa.dot.gov/bridge/steel/

Figure A.1 Examples of damage.

About the Joint Transportation Research Program (JTRP)

On March 11, 1937, the Indiana Legislature passed an act which authorized the Indiana State Highway Commission to cooperate with and assist Purdue University in developing the best methods of improving and maintaining the highways of the state and the respective counties thereof. That collaborative effort was called the Joint Highway Research Project (JHRP). In 1997 the collaborative venture was renamed as the Joint Transportation Research Program (JTRP) to reflect the state and national efforts to integrate the management and operation of various transportation modes.

The first studies of JHRP were concerned with Test Road No. 1—evaluation of the weathering characteristics of stabilized materials. After World War II, the JHRP program grew substantially and was regularly producing technical reports. Over 1,600 technical reports are now available, published as part of the JHRP and subsequently JTRP collaborative venture between Purdue University and what is now the Indiana Department of Transportation.

Free online access to all reports is provided through a unique collaboration between JTRP and Purdue Libraries. These are available at: http://docs.lib.purdue.edu/jtrp

Further information about JTRP and its current research program is available at: http://www.purdue.edu/jtrp

About This Report

An open access version of this publication is available online. This can be most easily located using the Digital Object Identifier (doi) listed below. Pre-2011 publications that include color illustrations are available online in color but are printed only in grayscale.

The recommended citation for this publication is:

Wang, Y., & Thrall, A. P. (2019). *Assessment of bridges subjected to vehicular collision* (Joint Transportation Research Program Publication No. FHWA/IN/JTRP-2019/01). West Lafayette, IN: Purdue University. https://doi.org/10.5703/1288284316870